

Thermodynamic Analysis: The Biphasic Nature of the DEAD-box RNA helicase Rok1p

Robert Miller Carlisle II

April 15, 2011

Biochemistry

Thermodynamic Analysis: The Biphasic Nature of the DEAD-box RNA helicase Rok1p

Robert Miller Carlisle II

A senior comprehensive project in partial fulfillment of the requirements for a bachelor of science degree from Allegheny College

I hereby recognize and pledge to fulfill my responsibilities, as defined in the Honor Code, and to maintain the integrity of both myself and the College community as a whole:

Approval by Senior Thesis Committee

Dr. Ivelitza Garcia

Dr. Margaret Nelson

Dr. Mark Ams

Table of Contents

Acknowledgements	**4**
Abstract	**5**
Introduction	**6-26**
Methods	**27-32**
Results	**33-50**
Conclusion	**51-54**
Appendix	**54-55**
References	**55-57**

Acknowledgments

I would like to thank my family for all the support they have given me not only in the past four years, but throughout my entire life. Thank you to my mom and dad for always being there for me when I needed you. I am extremely blessed to have parents as loving, caring, and amazing as you two. Thank you to my fiancé Miranda. You have been with me through good and bad times and I look forward to spending the rest of my life with you. CJ, I am so glad you and I have gotten closer over the past four years. I love you all very much.

Thank you also to my grandparents who have helped support me through college. It was always a pleasure to look into the stands and see you guys there cheering me on. I am very lucky to have grandparents as involved with my life as you. I pray that Papa smiles down upon me as I continue life's journey; may he rest in peace.

I would also like to extend a thank you to my housemates. Keith, Bucky, T, Tommy, and Dave, have become my best friends. I feel honored to have shared so many memories with them over the past four years. I wish them all good luck in their future endeavors and hope to share more good times in the future.

Thank you to all the faculty and administration who have helped me become the man I am today. Your engaging teaching style and your willingness to help me learn have pushed me to achieve more. There is no doubt in my mind that Allegheny College was the right place for me.

I cannot begin to express my gratitude towards Dr. Garcia. Thank you for everything you have done for me over the past year and a half. I am so glad that I was able to comp with such a great advisor and group of people. I cannot tell you how much I appreciate all the support and guidance you have given me for this project. I thoroughly enjoyed my time working on it and I wish you and your family well. Thank you to Michael and Erin for being so welcoming and helpful. You two are both great people and I know you will both succeed at whatever you do. I will never forget the fun we have had together working on our comps.

Abstract

RNA must fold into distinct and dynamic structures in order to function in the cell. In many cases, proteins are recruited to aid in RNA folding and refolding. For example, DEAD-box proteins are putative RNA helicases that utilize the energy of ATP binding and hydrolysis to disrupt hydrogen bonding in RNA. A large majority of DEAD-box proteins exhibit a substantial enhancement in ATP hydrolysis activity upon RNA binding. Stimulation of ATPase activity is facilitated by the conversion of a disorder to an ordered ATP binding site. However, Rok1p, a DEAD-box protein associated with early ribosomal assembly in *S. cerevisiae*, has proven to be RNA independent. This observation suggests that the protein is capable of adopting an ordered conformation in the absence of RNA binding. An Erying analysis was performed by monitoring the ATPase activity over a range of 10°C to 38°C to determine the thermodynamic parameters of the transition state in an effort to understand the disordered/ordered nature of Rok1p. These experiments showed that the RNA independent activity of Rok1p dramatically decreases as the temperature increases due to the entropic component of the protein. Our analyses support the hypothesis that Rok1p takes part in a disordered-ordered equilibrium; where, at low temperatures the protein favors the ordered conformation. The data also support the hypothesis that in the presence of RNA, Rok1p exists in two distinct catalytically competent conformations which have two separate rate limiting steps. A similar analysis was performed with Dbp3p, a DEAD-box protein associated with late ribosomal assembly in *S. cerevisiae*, to determine if these behaviors are general characteristics of DEAD-box proteins. It appears that in the absence of RNA, Dbp3p does not take part in a disordered-ordered equilibrium like Rok1p; rather it favors the open disordered state. This suggests that in the absence of RNA, the disordered-ordered equilibrium is unique to Rok1p. Further analysis of Dbp3p in the presence of RNA is required before it can be determined if the biphasic nature of Rok1p is common to all DEAD-box proteins.

Introduction

RNA Folding and Processing

All the necessary genetic information for life is contained in the macromolecule deoxyribonucleic acid (DNA). This nucleic acid is composed of heterocyclic bases, a sugar ring, and phosphate groups (see Figure 1A). Another important nucleic acid is ribonucleic acid or RNA. There are three key structural differences between DNA and RNA: nucleotide preference, 2' sugar position, and chemical variability. Although these two macromolecules have three nucleotides in common, adenosine, guanine, and cytosine, only RNA possesses uracil (see Figure 1B). Due to proofreading issues caused by deamination of cytosine to uracil, DNA possesses thymine not uracil. Another major difference between DNA and RNA is the sugar. The 2' position is occupied by hydrogen in DNA and a hydroxyl group in RNA (see Figure 1C). This 2'-OH group is also partly responsible for the structural variability of these two nucleic acids. Due to steric hindrance at the 2' position, RNA can only take on the helical secondary structure of a short A-form duplex (~10 base pairs) while DNA is found mostly in the B-form due to its thermodynamic stability (Figure 1D).

Furthermore, the single stranded nature and short helical regions of RNA allows it to make much more complex structures than double stranded DNA. RNA can form multiple secondary structures such as bulges, internal loops, junctions, hairpins, and previously mentioned A-form helices. These secondary structures provide single stranded regions utilized for scaffolding of tertiary structures. Unlike DNA, RNAs have many essential cellular functions based on their capability to form distinct and dynamic structures.[1]

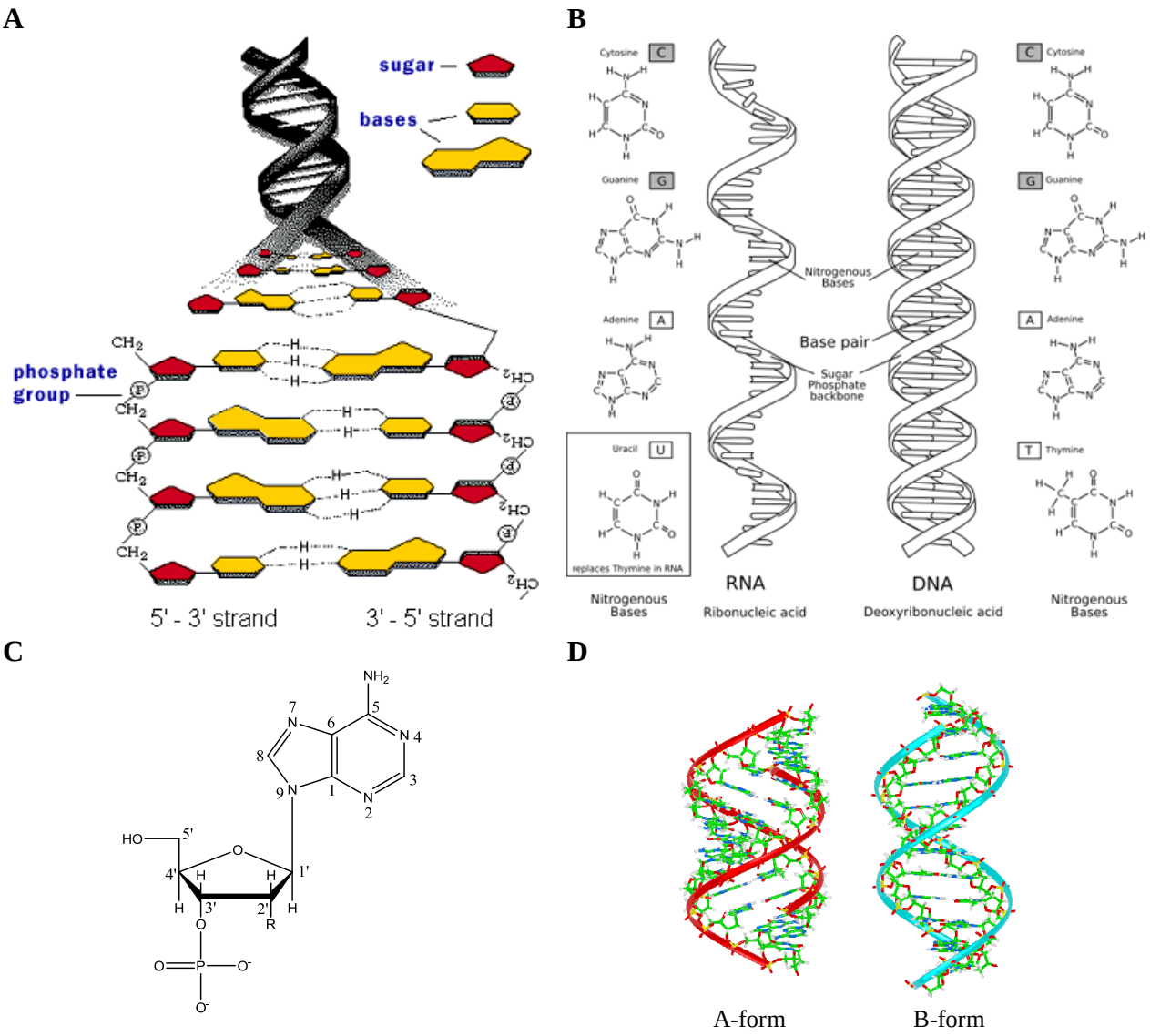


Figure 1: (A) Depiction of DNA structure. The two strands of DNA form a right-handed B-form double helix. The base, sugar, and phosphate group collectively form a nucleotide. This figure was taken from [2] and modified. (B) Comparison of DNA and RNA structure. This figure was taken from [3]. (C) Nucleotide example of DNA (deoxyribose sugar R=H) and RNA (ribose sugar R=OH). (D) Illustrations of helical forms. These particular representations are depicted with DNA. This image was modified from its original version.[4]

For example, tRNA shuttles amino acids to the ribosomes for protein synthesis. This RNA forms four distinct segments that interact to resemble an inverted "L". This structural feature provides a site for the covalent attachment of a specific amino acid and recognition by the ribosome. Ribosomes are responsible for protein synthesis inside a cell and they are also

composed of RNA (rRNA). The universal large and small subunits of ribosomes, as well as tRNA, are formed with the help of proteins and other cofactors.[1] As the primary sequence of the RNA interacts with itself, it begins to fold into secondary and eventually tertiary structures. This process can occur via multiple pathways and often get trapped in non-active intermediate structures(Figure 2).[5,6] Specific binding proteins can force RNA into its native or active state. RNA chaperones, a non-specific protein that prevents or reverses misfolding, can also guide an inactive folding intermediate to its active folding conformation (Figure 2).[5,6]

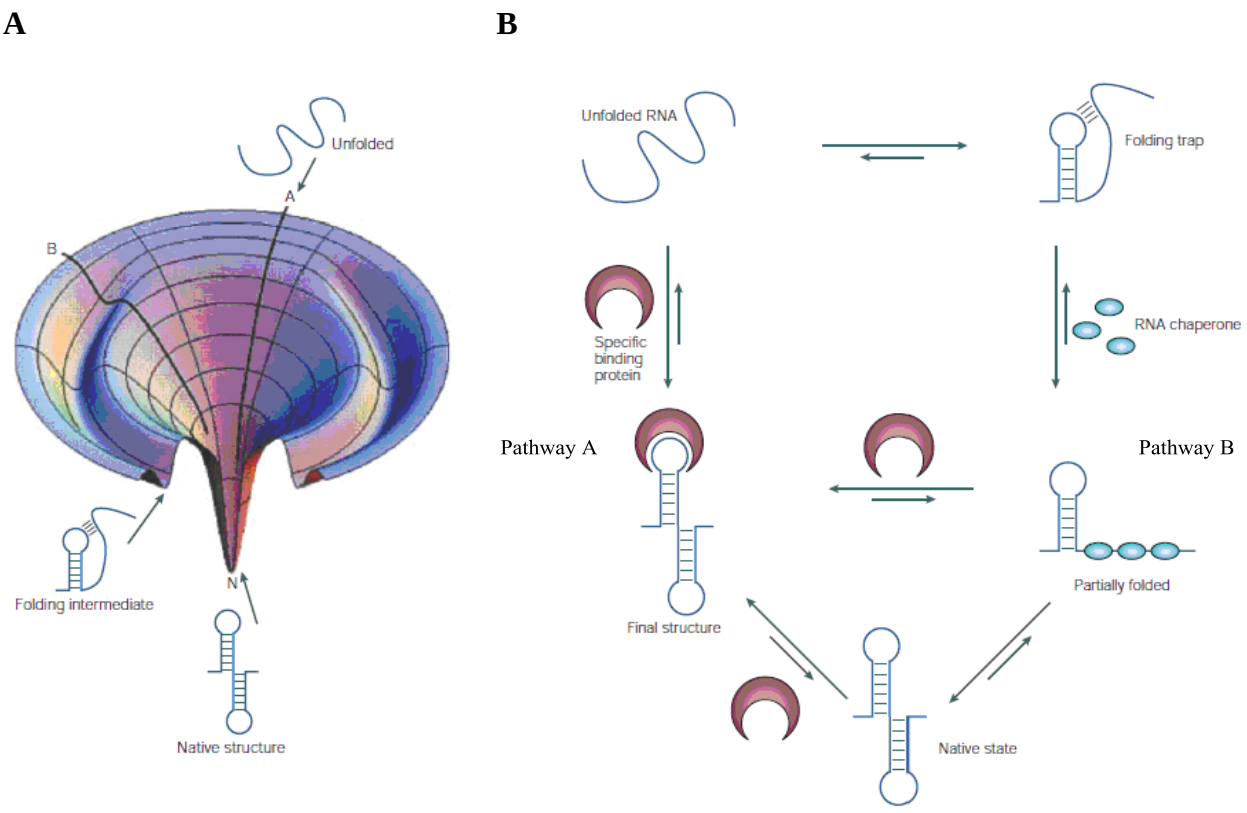


Figure 2: A free energy funnel representing various pathways for RNA folding. (A) The unfolded RNA can use specific binding proteins (pathway A) to fold directly into its native (N) structure. RNA chaperone proteins can reverse the conformation of a folding intermediate and guide the correct folding to the native structure (pathway B). (B) Pictorial representation of pathways A and B.[5]

Proteins are ubiquitous in nature. Not only are proteins involved with folding of RNA, but they are engaged in every biological process excluding information storage. Twenty amino acids make up the building blocks of a protein polymer. They are categorized by their specific functional groups: aromatic, nonpolar, polar, acidic, and basic. The structure and function of the particular protein is determined by a multitude of intermolecular forces. Hydrogen bonds, electrostatics, and hydrophobic interactions dictate the structural aspects of the protein including enzymatic active sites, binding pockets, and other protein-protein relationships. These interactions can also create substrate specificity. For example, a unique C-terminal domain on the *E. coli* helicase, DbpA, restricts its binding ability to the specific hairpin on the 23S rRNA.[7,8]

A helicase is an enzyme that catalytically unwinds double-stranded nucleic acids by utilizing the energy released from hydrolysis of nucleotide triphosphates (Figure 3).[9] Currently, five superfamilies have been defined, containing both DNA and RNA helicases, and use designations SF1-SF5. Although DNA helicases are vital for replication and other cellular processes this research will focus on RNA helicases proposing to aid RNA folding. The five superfamilies all exhibit domains that are folded very similar to RecA. The RecA protein is an ATP-dependent recombinase that mediates DNA strand exchange reactions by binding and hydrolyzing ATP.[10] Along with its folding pattern, RecA contains the Walker A and B motifs that are characteristic of a large majority of helicases.[11] SF3-SF5 possess one RecA-like domain with multiple conserved motifs across families. Unlike the three other super families, SF1 and SF2 are composed of dimers and monomers, possessing at least two RecA-like domains.[9]

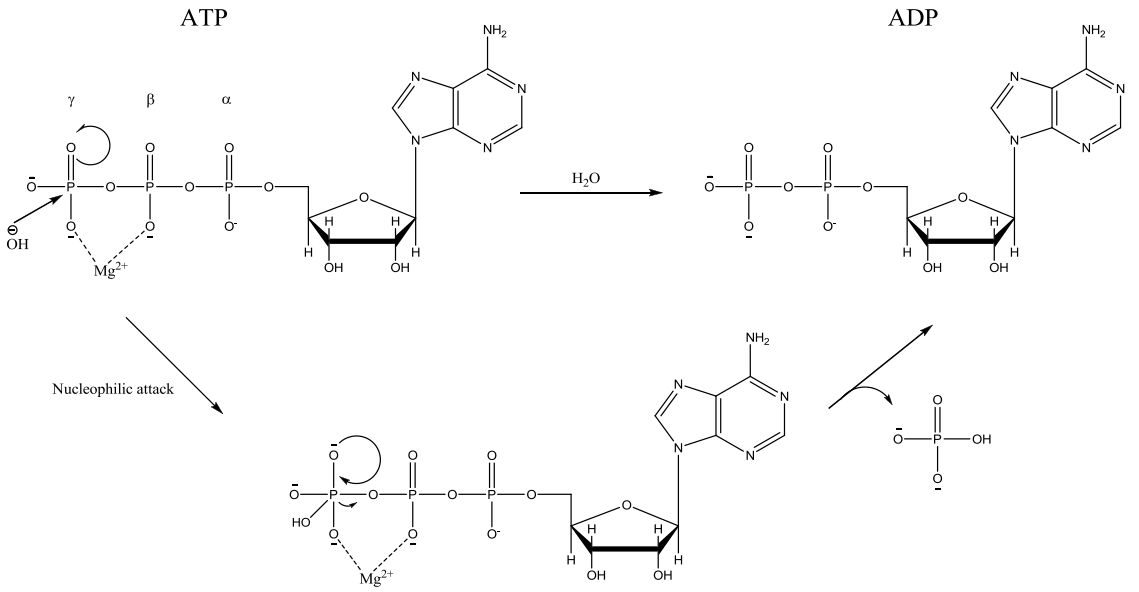


Figure 3: Mechanism of adenosine triphosphate (ATP) hydrolysis characteristic of RecA like domains. A water molecule is recruited to the active site by Mg^{2+} and deprotonated by an amino acid. The resulting hydroxide nucleophilically attacks the γ phosphorous, pushing the electron density onto the oxygen. The double bond between oxygen and phosphorous is reformed and ADP is released.

The largest sub-family in SF2 is known as the DEAD-box family. These DEAD-box proteins get their name from the Walker B motif which contains the following amino acids: Asp (D), Glu (E), Ala (A), and Asp (D).[1] Named after their discoverer, James E. Walker, the Walker A and B motifs, are a series of conserved amino acids responsible for facilitating the binding and hydrolysis of nucleotides in many proteins.[12] Each DEAD-box protein contains nine conserved motifs and a 300 amino acid helicase core that consists of an adenosine triphosphate (ATP) binding cleft between two globular domains, each containing multiple β-sheets and α-helices, connected by a flexible linker (Figure 4 and 5).[1,9] Characteristic of all DEAD-box proteins is the location of the binding sites. ATP binds between the two RecA like domains and RNA binds to the bottom of both domains in close proximity to the RNA binding motifs. It is clear from Figure 4B that motifs Ia, Ib, IV, and V are interacting with the ssRNA while Q, I, II, and VI are binding

with the ATP analog. Two amino acids in Motif I (Walker A motif), Thr and Lys, form H-bonds with the α phosphate and water, respectively.[13] The Glu amino acid in the Walker B motif is responsible for the deprotonation of water and subsequent hydrolysis.[13,14,15,16] His (motif VI) and Gly (motif V) also hydrogen bond to the water molecule.[13] Whereas, motifs IV and V are also involved with phosphate and sugar interactions. The two Arg residues in motif VI interact with the α, β, and γ phosphates while Asp in motif V hydrogen bonds to the 3'ribose hydroxyl.[13] The positively charged Arginines also help stabilize the ATP hydrolysis transition state.[17,18] The Q motif's Phe residue participates in π-stacking with the nitrogenous base while the Glu amino acid hydrogen bonds to nitrogen 6 and 7.[1] With the exception of motif III, the remaining conserved portions interact with the RNA backbone via hydrogen bonds and ionic interactions.[13] The hinge motif III is a flexible linker that allows the protein to "breathe" or transition between open and closed states.[9] The combination of ATP and RNA binding permits the core domains to switch from an open to closed conformation. Changes in the conformations are powered by the ATP binding and hydrolysis. Outside the 350-400 amino acid core, most DEAD-box proteins contain N- and C-terminal extensions involved in RNA targeting and protein recruitment.[9]

A **B**

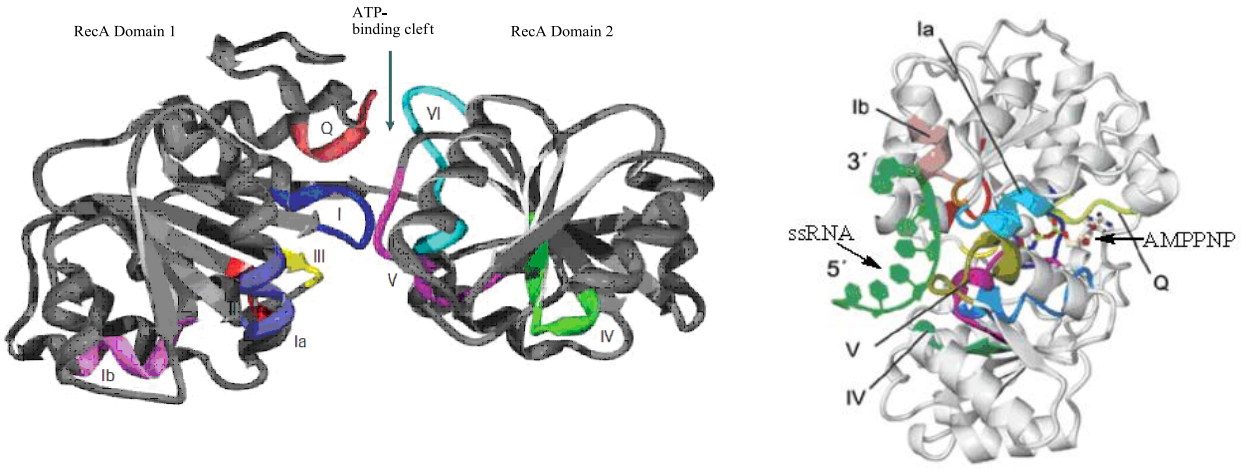


Figure 4: (A) Structure of the *Methanococcus jannaschii* DEAD-box protein. The conserved motifs are color coded to correspond with Figure 5.[1] This figure was taken from [1] and modified. (B) *Drosophila* Vasa DEAD-box protein rotated 90° clockwise with respect to A. The protein is expressed in the germline of higher eukaryotes possibly for differentiation purposes. It is shown here bound with ssRNA and a non-hydrolyzable form of ATP (AMPPNP). This figure was taken from [13] and modified.

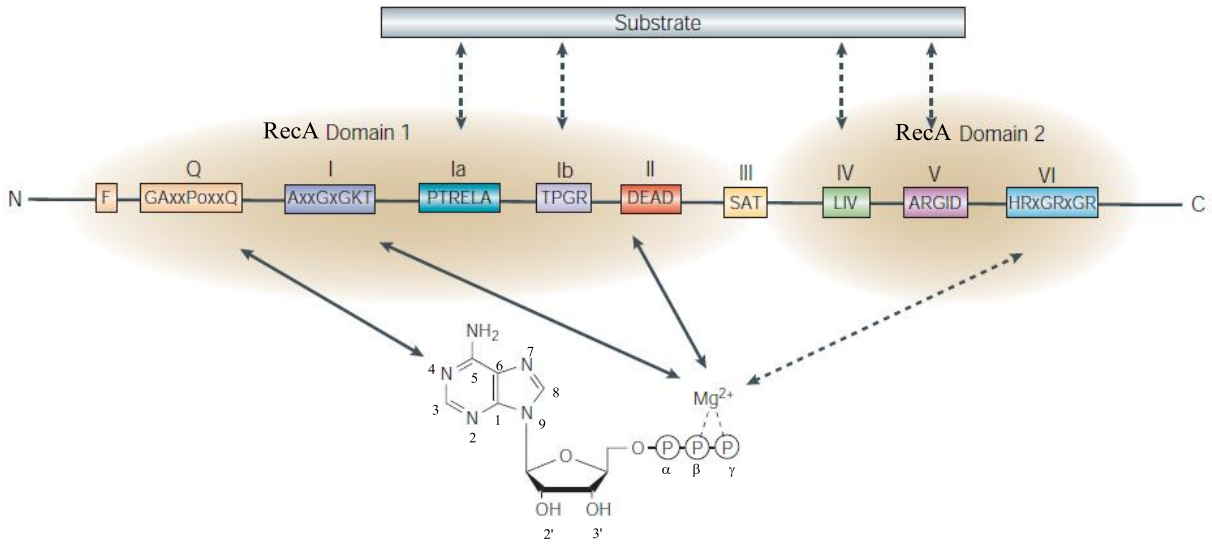


Figure 5: Conserved motifs in the DEAD-box family of proteins. Motifs Q, I, II, Vand VI interact with ATP while motifs Ia, Ib, IV, and V facilitate RNA (substrate) binding. The color schemes coordinate with the highlighted regions in Figure 4A. The 'o' represents Q, S, or T amino acids while the 'x' is representative of any amino acid. The figure was taken from [1] and modified.

Currently, there are multiple models of helix unwinding for specific helicase sub-families. RNA helicases use the energy released from ATP hydrolysis to unwind dsRNA (double stranded RNA).For example, RNA helicases can move along a strand of RNA 3'→5' or 5'→3' which results in the unzipping of helices. However, the DEAD-box proteins eIF4A and p68 do not show directional preference.[1] In addition, DEAD-box proteins are generally non-processive which indicates that they do not translocate or move along RNA. Although there are multiple mechanisms explaining helicases, the destabilization mechanism best explains the characteristics of DEAD-box proteins (see Figure 6 below). The destabilization model, like other proposed helicase models, begins with the binding of ATP and RNA. The actual unwinding process is not fully understood, but two probable pathways have been proposed. Pathway (a) utilizes the energy released via ATP hydrolysis to cause a conformational change within the protein, thus bending the RNA. This bending motion disrupts base pairings and causes the dsRNA to unwind. In this pathway, the protein freely dissociates from the RNA. The energy used to interrupt the RNA base pairs in pathway (b) is derived from the binding of ATP.[9,13] As the protein goes through its conformational change from open to an ATP bound closed state, the steric hindrance resulting from α-helix 7 located near motif Ib of the protein causes the RNA base pairs to unzip.[13] The protein uses the energy obtained from hydrolysis to dissociate from RNA. For both pathways, whether or not the base pairs reconnect or further unzip depends on the overall stability of the remaining dsRNA.[9,13] Thus, DEAD-box proteins are frequently referred to as putative RNA helicases. A large number of *in vitro* studies do not show helicase activity. This phenomenon could be attributed to internal cellular environments that cannot be replicated in a lab setting or *in vitro* experiments may be lacking other necessary proteins and cofactors. However, most DEAD-box proteins exhibit RNA-dependent ATPase activity while some show RNA-

independency. The relative rates at which a certain protein performs its ATPase activity can provide information about its catalytic capacity. The eIF4A DEAD-box hydrolyzes ATP at a rate of 3 min^{-1} whereas the Ded1p has a rate of 600 min^{-1}.[9] This suggests that similar core structures show the ability to tune the hydrolysis of ATP levels which are necessary for function.[19]

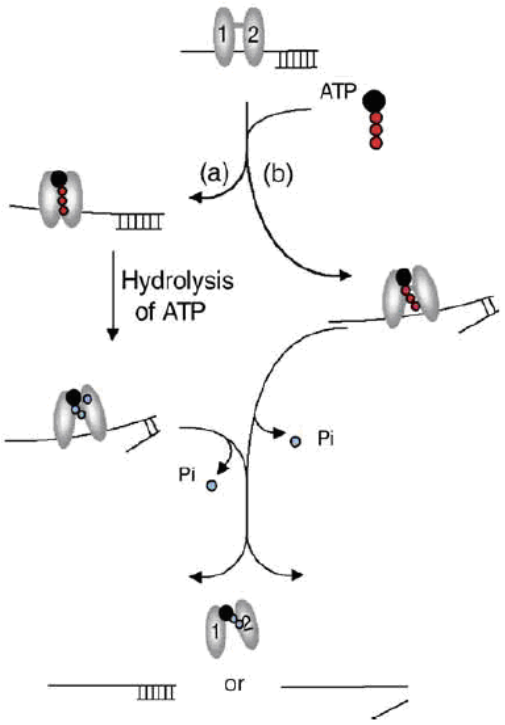


Figure 6: Depiction of the destabilization model. Upon hydrolyzing ATP, the protein undergoes a conformational change that causes the dsRNA to unwind (pathway (a)). The binding of ATP and subsequent closed conformation provides the energy to destabilize the dsRNA (pathway (b)). This figure was taken from [9].

The ability to fold and modulate dynamic RNA structures is a very valuable tool in a number of RNA mediated cellular processes. Due to their unwinding ability, DEAD-box proteins are crucial in most RNA metabolic processing pathways. Interestingly, 45% of RNA helicases in Eukaryotes are dedicated to ribosome biogenesis. The ribosome is a large protein-RNA complex that involves 4 RNAs totaling 6980 nucleotides and 83 proteins. A mature ribosome, comprised of a large 60S and small 40S subunit, is used in protein synthesis. The 60S large subunit stems from three rRNA: 5S, 5.8S, and 25S. The 18S rRNA forms the 40S small subunit. The S refers to

the sedimentation constant which is proportional to the weight of the RNA. Assuring the proper folding of ribosomal RNA is extremely important because it is the catalytic subunit in the translational process. Studies have shown that misprocessing of the ribosome can lead to diseases such as Dyskeratosis congenital and cancer.[20,21,22] Cancer treatments have also focused their attention on inhibiting ribosomal biogenesis.[23,24]

The process of eukaryotic ribosomal biogenesis is conserved and *Saccharomyces cerevisiae* (baker's yeast) is widely studied as a model for processing.[25] The production of ribosomes takes place in the nucleolus of the cell, a sub-compartment of the nucleus. The locus for the four previously mentioned rRNAs is a rDNA (ribosomal DNA) repeat on chromosome XII (see Figure 7 below). The 9.1 kilobase rDNA unit is repeated upwards of 200 times on the long arm of the chromosome. The DNA repeat produces a 35S pre-RNA and 5S pre-RNA. The 35S pre-RNA is transcribed by RNA polymerase I and contains the 18S, 5.8S, and 25S mature rRNA. The 5S pre-RNA is transcribed separately by RNA polymerase III and is responsible for the mature 5S rRNA.

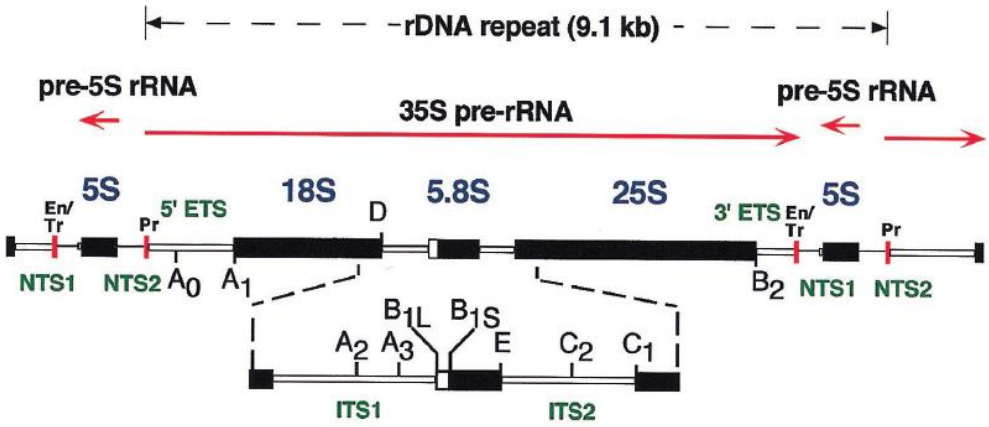


Figure 7: Pre-rRNA processing. The promoter (pr), terminator (tr), and enhancer (eh) refer to sequences on the operon that encodes the pre-rRNA transcript. Each pre-rRNA transcript has internal (ITS) and external (ETS) transcribed spacers to separate the mature rRNAs (solid black boxes). These spacers are depicted as white boxes while nontranscribed spacers (NTS) are represented as single black lines. During processing, the spacers will be cleaved at their designated sites. This figure was taken from [25] and adapted.

Maturation and modification of the 35S and 5S pre-rRNA follow distinct pathways. The pre-5S rRNA transcript undergoes minor modifications and few cleavages; therefore its maturation process is kinetically faster than that of the 35S transcript. The 35S pre-rRNA requires more processing due to the internal transcribed spacers (ITS1 and ITS2) and external transcribed spacers (3' ETS and 5' ETS). These spacers provide the necessary room for protein factors to ensure appropriate cleavage and folding. The maturation process requires three major accessory factors. Endo- and exonucleases cleave the RNA spacers at specific internal and terminal sites (see Figure 8, blue factors). Small nucleolar ribonucleoprotein particles (snoRNP), RNA-protein complexes, chemically modify rRNA for structure stability and folding (see Figure 8, black factors).[25] Finally, DEAD-box proteins are proposed to modulate rRNA structure and/or recruit other processing factors (see Figure 8, red factors).[26]

Removal of the 3' non-transcribed spacer from the 5S pre-RNA provides the mature 5S rRNA. Whereas, the 35S pre-RNA is initially cleaved at the A_0, A_1, and A_2 sites by nucleases.

The resultant 20S pre-RNA is cleaved at site D to yield the mature 18S rRNA. The $27SA_2$ pre-RNA can be matured via two pathways. Approximately 85% of the $27SA_2$ pre-RNA is modified at sites A_3 and B_{1S} successively while the other 15% of mature 5.8S and 25S rRNA stem from cleavage at sites B_{1L} followed by modification at sites B_1 and B_2 (Figure 8). DEAD-box proteins are utilized at multiple points throughout the process to ensure proper RNA structure and folding. Studying DEAD-box proteins associated with ribosome biogenesis will unveil intricate details of their specific roles in this important process. Knowledge gained through biochemical studies can lead to advanced cancer therapies and treatments for other diseases related to protein synthesis.[25]

For example, Rok1p is a DEAD-box protein involved in an early step of rRNA processing. Studies have shown that Rok1p is closely associated with snR10, a snoRNP involved in the psuedouridylation, or ψ modification, of uracil via base rotation of the 25S rRNA (see Figure 9).[25,27] Genetic depletion of Gar1p, another protein associated with snR10, inhibits pre-rRNA processing, specifically the cleavages at sites A_0, A_1, and A_2.[25,27,28,29] Similarly, the deletion of Rok1p affects the cleavage of the first three sites suggesting that Gar1p and Rok1p interact. The observed phenotypes may be a result of a decrease in the ability of snR10 to attach and dissociate from the pre-RNA due to the absence of Rok1p.[28]

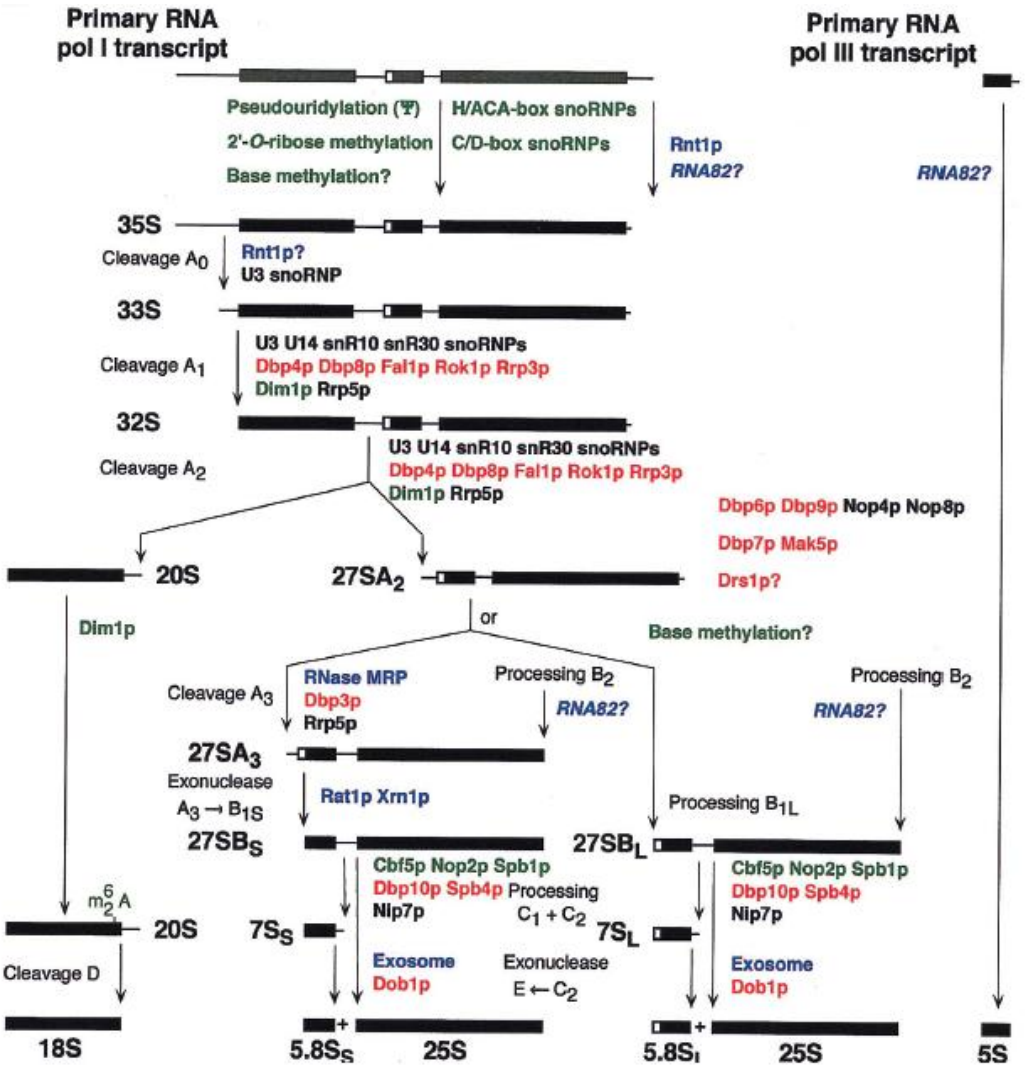


Figure 8: pre-rRNA processing in *S. cervisiae*. The colors are representative of the type of protein trans-acting factor. Green corresponds to components involved in pre-rRNA modifications. Endo- and exonucleases are depicted as blue while snoRNPs are shown in black. The red factors are DEAD-box proteins. This figure was taken from [25] and modified.

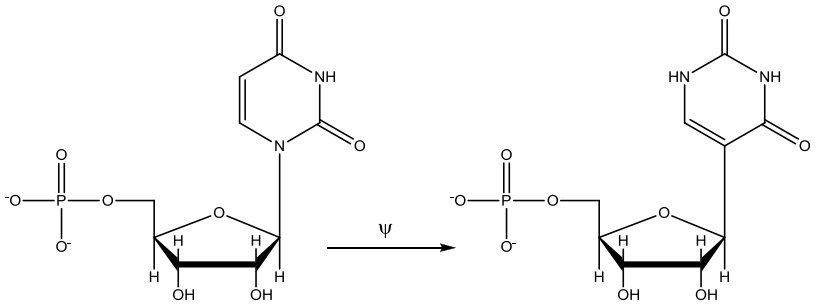


Figure 9: Transformation of uracil via ψ modification.

Biochemical Characteristics of Rok1p

Rok1p was extensively characterized with respect to three other yeast ribosomal proteins. Although Rok1p can bind multiple nucleotide triphosphates, ATP is the only one capable of providing the energy necessary for rRNA processing.[30] In the presence of RNA, Rok1p exhibits a k_{cat} of 15 ± 5 min^{-1}, K_M(ATP) of 1.1 ± 0.3 mM, and a K_{app}(RNA) of 7 ± 3 nM. When comparing Rok1p's catalytic rate constant with other DEAD-box proteins, it falls on the lower end of the spectrum. The *in vitro* catalytic rates for DEAD-box proteins range from 3 min^{-1} for eIF4A to 600 min^{-1} for DbpA.[1] The K_M and K_{app} refer to the equilibrium binding constants of ATP and RNA, respectively. Rok1p binds ATP comparable to other rRNA processing proteins like Dbp3p (1.3 ± 0.7 mM) and Rrp3p (2.4 ± 0.4 mM) while Dbp4p binds the trinucleotide much tighter (0.24 ± 0.09 mM).[30] DEAD-box proteins also bind RNA, but much tighter than ATP. The three previously mentioned DEAD-box proteins possess a K_{app} ranging from 0.6 to 6 nM.[30] These values are very comparable to other DEAD-box proteins: Dbp3p (1.3 ± 0.7 mM) and Oligomer length studies revealed that Rok1p's RNA binding site requires a single stranded RNA approximately 90 nucleotides long, significantly larger than most other helicases. This suggests that Rok1p might prefer dsRNA and its binding could be assisted by the non-conserved N- and C-terminal.[19,30] An in depth look at the pH profile of Rok1p revealed some interesting and unique characteristics. ATPase activity peaked around physiological pH (~7) (see Figure 10 below). Rok1p is stimulated 10-fold in the presence of RNA when a Mes buffer is utilized. However, under certain buffer conditions Rok1p shows no RNA stimulation. Interestingly, ATPase activity for most DEAD-box proteins is dependent on RNA where the activity of hydrolysis is stimulated ≥ 5-fold.[30] This observation is especially interesting considering the structural similarities

between the three buffers (Figure 10). The reason for these buffer effects is currently unknown.[30]

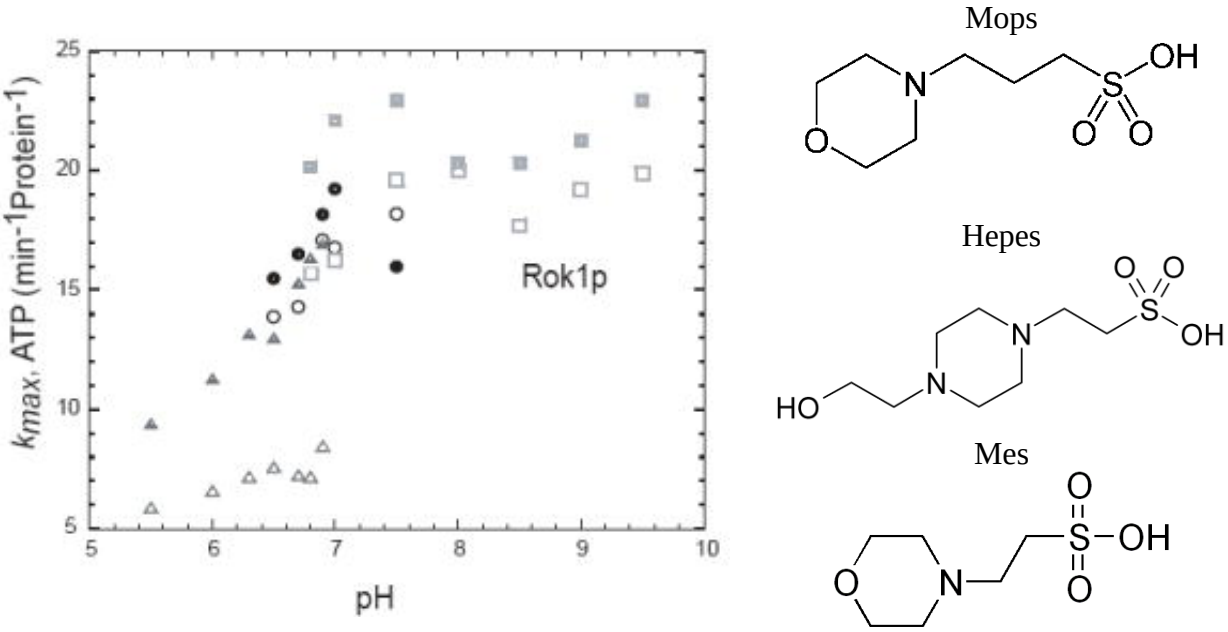


Figure 10: ATPase pH dependency. When Mops (circles) and Hepes (squares) buffers were utilized, Rok1p did not exhibit activity stimulation in the presence of RNA (shaded shapes) compared to the absence of RNA (clear shapes). There was some activity stimulation with Mes (triangles) buffer. This figure was taken from [30].

There are two main hypothesises regarding Rok1p's apparent RNA-independent nature. The first hypothesis is centered around the terminal domains. The N- and C-termini of multiple DEAD-box proteins have exhibited RNA binding characteristics.[30,31,32,33] It has been suggested that the flexible N- and C-terminal domains are mimicking RNA or stabilizing the closed conformation of the protein. As depicted in Figure 6, the protein is in a closed conformation when ATP and RNA are bound, but in an open conformation when one is not bound. Thus, removal of one or more of the peripheral domains may restore RNA dependence. Another hypothesis deals with a disordered-ordered equilibrium.[34] In general, DEAD-box proteins favor an open disordered conformation; therefore, RNA and ATP bind and shift the equilibrium toward the a closed ordered state (see Figure 11A below). However, the theory suggests that Rok1p

favors the closed ordered conformation. Thus, RNA binding does not stimulate hydrolysis as seen in other DEAD-box proteins (Figure 11B).

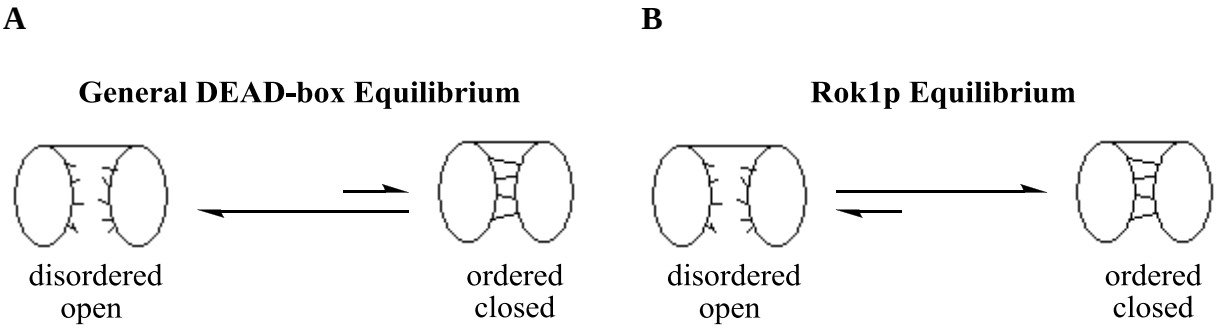


Figure 11: (A) Disordered-ordered equilibrium depiction. Most DEAD-box proteins prefer the open disordered state. (B) This theory suggests that Rok1p's RNA-independent nature is caused by its propensity to favor the closed ordered state.

The suggested equilibrium shift in Rok1p was directly observed in the DEAD-box protein SecA (see Figure 12 below).

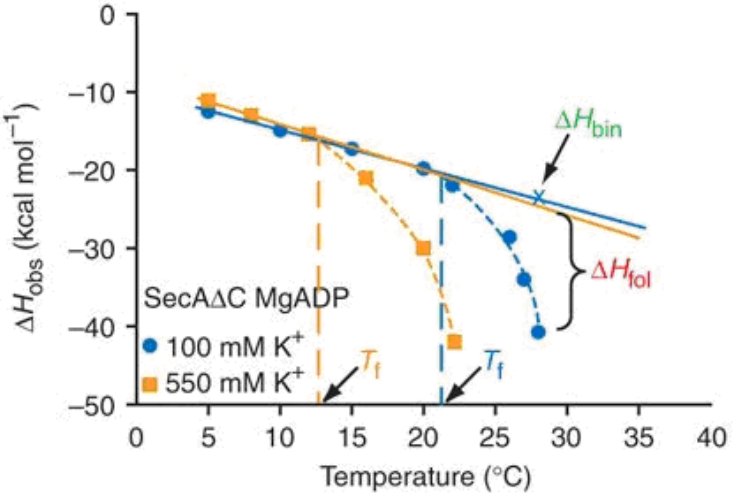


Figure 12: ΔH_{obs} of MgADP binding to SecAΔC as a function of temperature in 100 mM K^+ and 550 mM K^+ buffer. Broken lines represent fits to the higher temperature points. T_f is the temperature indicating disorder-order transition induced upon nucleotide binding. This figure was taken from [34].

As seen in Figure 12, the enthalpy of ADP binding (ΔH_{obs}) changes as a function of temperature. The ΔH_{obs} is negative, thus suggesting that intermolecular force formation

dominates. Specifically, for 100 mM K^+, ΔH_{obs} follows a linear pattern at lower temperatures representing a constant heat capacity (C). At approximately 21°C the enthalpy begins to decrease at a different rate, therefore, the heat capacity changes. The temperature dependent change in the heat capacity is consistent with a protein becoming more dynamic and disordered. Furthermore, increasing the ion concentration to 500nM K^+ decreased the temperature at which the disorder-order transition occurred. The increased salt concentration disrupts the protein's interaction between domains via electrostatic interactions. This causes the protein to populate the open disordered state at a lower temperature. Hence, these data suggest that a conformational equilibrium shifted towards a more disordered state is seen in the protein SecA.[34,35,36]

Similar thermodynamic analyses of Rok1p also suggest disordered-ordered equilibrium preference.[37] Generally, the rate of a reaction increases with increasing temperature. This increase in energy destabilizes the starting material which allows the activation energy barrier to be overcome faster, thus increasing the rate of a reaction. The relationship between the rate of a reaction and temperature is expressed using the Eyring equation (Equation 1).

$$\ln\left(\frac{k_{cat}h}{k_B T}\right) = \frac{-\Delta H^{\ddagger}}{R}\frac{1}{T} + \frac{\Delta S^{\ddagger}}{R} \qquad \text{Equation 1}$$

Where k_{cat} is the rate constant, h is Planck's constant, k_B is Boltzmann's constant, R is the gas constant, $\Delta H^{\ddagger}$ is the change in the enthalpy of the transition state, $\Delta S^{\ddagger}$ is the change in entropy of the transition state, and T is the temperature. The Eyring model relates the catalytic rate to a transition state equilibrium and views the transition state as an intermediate, facilitating the calculation of thermodynamic parameters.[38,39] In the absence of RNA, the catalytic rate increases as the temperature approaches 18°C. At the higher temperatures, the rate begins to steadily decrease (Figure 13).

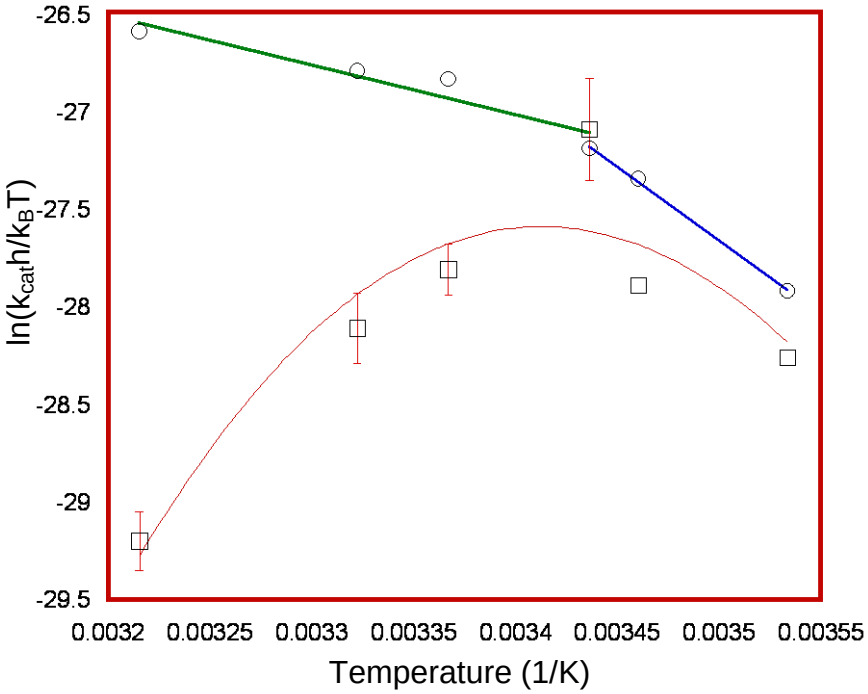


Figure 13: Combined Eyring plot of Rok1p in the presence (circles) and absence of RNA (squares). Error bars were produced for temperatures that had at least three trials. Data is from [37].

The decreasing reaction rates with increasing temperature in the absence of RNA provides a convex relationship for Rok1p.[38] The linear Eyring equation is not appropriate for the convex nature of Rok1p without RNA. The convex pattern suggests that the enthalpic and entropic components are temperature dependent. This dependence in temperature also suggests a change in the heat capacity similar to SecA. Therefore, the integrated Eyring equation incorporating a change in the specific heat capacity must be used to accurately assess the disordered-ordered equilibrium proposed for Rok1p (Equation 2; Appendix A).

$$\ln\left(\frac{k_{obs}h}{k_BT}\right) = \frac{-\Delta H^{\ddagger}(T_o)}{RT} + \frac{\Delta S^{\ddagger}(T_o)}{R} + \frac{\Delta C_p}{R}\left(-1 + \frac{T_o}{T} + \ln\left(\frac{T}{T_o}\right)\right) \qquad \text{Equation 2}$$

Where ΔC_p is the change in specific heat, T_0 is the reference temperature, and k_{obs} represents k_{cat}.

The modified Eyring equation yields the transition state thermodynamic parameters of Rok1p at each temperature (Table 1).[40]

Table 1: Thermodynamic parameters of Rok1p's transition state at specific temperatures. $\Delta G^{\ddagger}$ represents the Gibbs free energy of the transition state at the designated temperature. The data was taken from [37].

Temperature (°C)	$\Delta H^{\ddagger}$ (kJ/mol)	$\Delta S^{\ddagger}$ (kJ/mol K)	$\Delta G^{\ddagger}$ (kJ/mol)	$T\Delta S^{\ddagger}$ (kJ/mol)
10	79.20	0.05	66.2	14.6
16	30.40	-0.124	66.4	-35.8
18	14.20	-0.181	66.7	-52.7
24	-34.5	-0.346	68.3	-102.8
28	-67	-0.455	69.9	-136.0
38	-148	-0.720	75.8	-223.9

An evident temperature dependence of Rok1p emerges for all three major thermodynamic parameters: enthalpy, entropy, and free energy. The decreasingly positive $\Delta H^{\ddagger}$ from 10°C - 18°C hints towards a closed conformation (Table 1). Energy is being added to the system to possibly disrupt intermolecular forces to accommodate ATP within a preformed binding pocket at higher temperatures. The negative $\Delta H^{\ddagger}$ signifies that intermolecular force formation, most likely hydrogen bonds and ionic interactions, between the open Rok1p protein and ATP dominate consistent with the formation of an ATP binding pocket. The disordered-ordered facet of the equilibrium is truly elucidated from the $\Delta S^{\ddagger}$ trend. A negative $\Delta S^{\ddagger}$ means entropy is decreasing, the protein is becoming more ordered. The negligible change in the negative $\Delta S^{\ddagger}$ over the three lower temperatures indicates that the protein active site is becoming more ordered as it binds ATP and enters the transition state (Table 1). Although it is in a closed state, the binding of ATP creates a complex network of hydrogen bonds with the active site of Rok1p. The locking of functional groups in place and becoming more ordered during the transition state is consistent with a negative $\Delta S^{\ddagger}$. Furthermore, a dramatic decrease in $\Delta S^{\ddagger}$ at the higher temperatures is representative of Rok1p transitioning from a disordered open state to an ordered closed ATP bound state, thus drastically reducing entropy. The $T\Delta S^{\ddagger}$ component in the Gibbs free energy equation contributes more to the increasing Gibbs free energy than the $\Delta H^{\ddagger}$ at

higher temperatures (Table 1). This entropically driven process suggests a Rok1p disordered-ordered equilibrium in practice, similar to the equilibrium shown in SecA.

A closer look at the Eyring plot alludes to the possibility of Rok1p exhibiting different rate determining steps in the presence of RNA (Figure 13). The apparent break in data points at 18°C suggests a biphasic character for the catalytic step. Eyring plots utilizing two lines to fit the data illustrate two distinct rate determining steps possible from the protein existing in two distinct conformations that are both catalytically competent.[41,42,43,44,45,46] In order to ensure the biphasic nature of Rok1p, more trials were compiled at each temperature in order to determine the statistical variability of the k_{cat}.

Another main question that still remains; is this interesting behavior in the absence of RNA unique to Rok1p or is it a common trait among DEAD-box proteins? Examining Dbp3p, a yeast DEAD-box protein, will help answer this lingering question. Dbp3p interacts with the RNase MRP complex facilitating the cleavage of the $27SA_2$ pre-rRNA at site A_3 (Figure 9).[47] Deletion of Dbp3p is not lethal to 25S rRNA maturation. However, accumulation of the $27SA_2$ pre-rRNA has been shown to occur in the absence of Dbp3p; the maturation of the 25S rRNA proceeds at a much slower pace. An extensive kinetic analysis of Dbp3p revealed its parameters: $k_{cat} = 170 \pm 15\ min^{-1}$; $K_M(ATP) = 1.3 \pm 0.7$ mM; and $K_{app}(RNA) = 1.2 \pm 0.6$ nM.[30] Compared to Rok1p's previously mentioned kinetic parameters, Dbp3p is a much more efficient ATPase and yet binds the nucleotide with a similar affinity. Nevertheless, Dbp3p binds RNA almost six-fold tighter than Rok1p. Unlike Rok1p's unique activity associated with various buffers, Dbp3p was stimulated 10-fold upon the addition of RNA regardless of the buffer (Figure 14). However, Dbp3p does show substantial RNA-independent activity compared to other DEAD-box proteins, approximately 20 min^{-1}.[30]

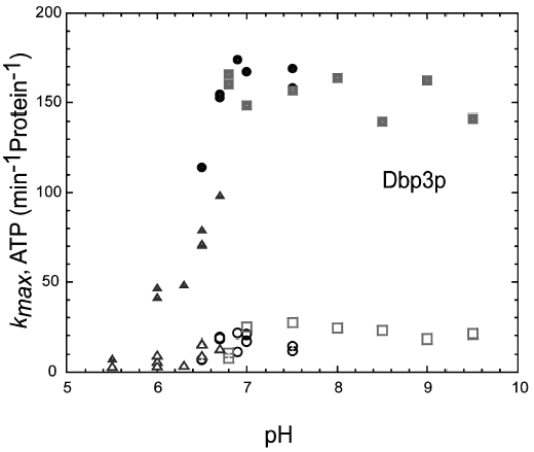


Figure 14: ATPase pH dependency of Dbp3p. Mops (circles), Hepes (squares), and Mes (triangles) buffers produced a large activity stimulation in the presence of RNA (shaded shapes) compared to the absence of RNA (clear shapes). There was still some activity (~20 min^{-1}) in the absence of RNA for all buffers. This figure was taken from [30].

Methods

Phosphate Detecting Agent

A 0.053% m/v malachite green solution was prepared monthly by combining 0.1325g of malachite green with 250mL of double deionized water (ddH_2O). A 0.21M ammonium molybdate solution was prepared monthly through the combination of 10.5g ammonium molybdate, 93mL 12.1M HCl, and 157.0 ddH_2O. The malachite green solution (6mL) and the ammonium molybdate solution (2mL) were combined in a 3:1 ratio. Tween-20 was also added to the mixture to a final concentration of 0.01%. The detecting agent was allowed to sit for at least an hour at room temperature in order for molybdate and malachite green to coordinate. Over this period of time the detecting agent changed color from a dark blue-green to a lighter yellow-green.

Phosphate Standard Curve

A phosphate standard curve was generated for every assay. A 1X Master Mix was prepared by combining 300µL 10X Master Mix (ddH_2O, 1.00% Tween-20, 0.5M Hepes, 0.25M KCl, 0.10M $MgCl_2$, 0.01M DTT; components added in order listed) in 3mL of ddH_2O. The 1X Master Mix (1mL) was combined with 1M K_3PO_4 (1µL) to form a 1mM phosphate solution. A 160µM phosphate solution was created from 840µL 1X Master Mix and 160µL 1mM phosphate solution. Using a 96-well plate, nine serially diluted phosphate solutions were made with the following concentrations (µM):160, 120, 90, 67.5, 50.6, 38, 28.5, 21.4, and 0. Using a 386-well plate, 20µL of each phosphate solution was mixed with 40µL phosphate detecting agent.

ATP Dilution

Eleven serially diluted ATP solutions in ddH_2O were made using a 96-well plate and ATP stock of various concentrations. The final 1X concentrations of each ATP solution in the reaction were as follows (mM): 5.6, 5.01, 4.01, 3.0, 2.0, 1.0, 0.7, 0.4, 0.3, 0.2, and 0.

1.25X Master Mix (-) RNA

The following were combined in a 2mL microcentrifuge to a total volume of 1500µL at a 1.25X final concentration: ddH_2O, 0.0125% of 25% Tween-20, 62.5mM Hepes, 31.2mM KCl, 12.5mM $MgCl_2$, 1.25mM DTT, and 336nM Rok1p. The components were added in the order listed. The presence of Tween-20 prevents Rok1p or the RNA from sticking to the sides of the wells or the microcentrifuge tubes. Hepes is a common buffer used for biochemical reactions at a neutral pH. Potassium and chloride help stabilize charges on Rok1p as well as RNA. Although magnesium helps stabilize charges as well, its main role is the recruitment of H_2O to the active site of Rok1p. Similarly, the concentration of RNA was in saturating conditions. Disulfide bonds are dissolved by dithiothreitol (DTT) to ensure an active protein.

1.25X Master Mix (+) RNA

The following were combined in a 2mL microcentrifuge to a total volume of 1500µL at a 1.25X final concentration: ddH_2O, 0.0125% of 25% Tween-20, 62.5mM Hepes, 31.2mM KCl, 12.5mM $MgCl_2$, 31.3nM *S. cervisiae* rRNA, 1.25mM DTT, and 336nM Rok1p. The components were added in the order listed.

ATPase Assay-Rok1p

The 88 wells of a 384-well plate involved with the reactions were each filled with 5µL of 0.5M Ethylenediaminetetraacetic acid (EDTA) and centrifuged for 1 minute at 3500rpm. The reaction is quenched by the coordination of Mg^{2+} to EDTA; ATP hydrolysis ceases without the

ability to recruit water to the active site. Thus EDTA is in excess of Mg^{2+} to ensure the reaction is quenched; EDTA concentration (1X=125mM) is more than 16 fold greater than Mg^{2+} concentration (1X=7.5mM). Aliquots (112μL) of 1.25X Master Mix (+ or – RNA) were added to eleven microcentrifuge tubes. After being incubated at the reaction temperature (10, 16, 18, 24, 28, or 38°C) for 5 minutes, a 28μL aliquot of each serially diluted solution of ATP was added and a timer was started immediately. A 15μL aliquot was taken from each of the eleven reaction mixtures and was transferred to the wells containing EDTA at the appropriate time points for (+) RNA reactions based on the reaction temperature: 2 minutes for 10 and 18°C and 1.5 minutes for the remaining temperatures. After all 8 time points passed, 20μL of each serially diluted phosphate standard solution was added to the 384-well plate. The serially dilute phosphate solutions along with all 88 wells containing reaction mixture were mixed with 40μL of phosphate detecting agent. The 384-well plate was centrifuged for 1 minute at 3500rpm and then absorbance readings were taken at 650nm. After a 15 minute incubation period at 35°C and 5 minute incubation period at room temperature, the absorbance readings at 650nm were taken again. Following a 10 minute incubation at 35°C and 5 minutes at room temperature, the absorbance readings at 650nm were taken for a third time. The 10 minute incubation at 35°C and the 5 minute at room temperature was repeated before obtaining a final set of absorbance readings at 650nm. Multiple incubations were performed in order to obtain data for all reactions; the lower concentrations required more time to display a detectable color change. The first incubation allowed the rates for the higher ATP concentrations to be elucidated while the two subsequent incubations revealed the rates for the lower ATP concentrations.

ATPase Assay-Dbp3p

The same procedures were carried out for Dbp3p assays with a few modifications. In order to keep concentrations of all components consistent with the Rok1p assay, 80% glycerol was added to the (+) RNA 1.25X Master Mix with a 1.25X final concentration of 250mM. The order of addition was also changed for (+) RNA 1.25X Master Mix such that the last three components added were 80% glycerol, Dbp3p, and RNA, respectively. The time points used for the Dbp3p assays in the absence of RNA were as follows: 2 minutes for 10 and 16°C, 1.75 minutes for 18°C, and 1.25 minutes for the remaining temperatures. The only known time point for Dbp3p assays in the presence of RNA is 1.25 minutes at 10°C. Because Dbp3p reactions are faster, shorter time points are necessary to capture the appropriate kinetic data. Considering the relative rates of the two proteins this seems logical: Dbp3p boasts a k_{cat}~$30min^{-1}$ in the absence of RNA, while even in the presence of RNA, Rok1p only displays a k_{cat} value of approximately $20min^{-1}$. The incubation schedule was adjusted in order to obtain data for the higher concentrations. Dbp3p reaches saturation faster because it has a much higher catalytic rate constant than Rok1p; therefore, more absorbance readings were required to obtain data. Absorbance readings were still taken at 650nm immediately following centrifugation. The 384-well plate was subjected to three 5 minute incubations at 35°C. After each incubation period the absorbance readings were taken at 650nm except for the third incubation after which the well plate was incubated at room temperature for 5 minutes before having the absorbance readings taken at 650nm. The well plate was incubated two cycles for 10 minutes at 35°C and 5 minutes at room temperature. After each cycle the absorbance readings were taken at 650nm.

Data Analysis

The absorbance readings were converted into amounts of phosphate present in each well. This was accomplished using Beer's Law and values from the phosphate standard calibration curve, specifically the slope and y-intercept (Scheme 1).

$$A = \varepsilon \left(\frac{nmol\ PO_4^{-3}}{\mu L}\right) l + constant \Rightarrow$$

$$y = mx + b \Rightarrow$$

$$A = m\ (nmol\ PO_4^{-3}) + b \Rightarrow$$

$$(nmol\ PO_4^{-3}) = \frac{(A - b)}{m}$$

Scheme 1: Beer's Law can be represented as a linear equation for the phosphate standard curve. The slope includes amount of PO_4^{-3}, molar absorbtivity (ε), path length (l), and volume. Since the light was directed up through the well and not across a fixed boundary, the path length was proportional to the volume in the well. A rearrangement of the slope equation and values inputted from the phosphate standard curve determined the amount of phosphate present in each well where the where absorbance represented by A, slope by m, and the constant by b. Since zero phosphate represented a constant non-zero absorbance, a constant was necessary.

The amounts of PO_4^{-3} in each well were plotted against time. The slope of the lines corresponded to nmol PO_4^{-3}/min which were converted to the rate through a series of unit conversions (Scheme 2).

$$\left(\frac{nmol\ PO_4^{-3}}{min}\right)\left(\frac{1\ mol\ PO_4^{-3}}{1\ x\ 10^9 nmol\ PO_4^{-3}}\right)\left(\frac{1}{60\ x\ 10^{-6}L}\right)\left(\frac{1L}{270\ x\ 10^{-9} mol\ Rok1p}\right)=\left(\frac{M\ PO_4^{-3}}{(min)(M\ Rok1p)}\right)$$

Scheme 2: Calculation of observed reaction rate. The final reaction volume was 60µL and the concentration of Rok1p was 270nM for every reaction. Although the final reaction volume was the same, the final concentration of Dbp3p was 50nM.

The rates obtained after the incubations for each reaction were averaged. The average observed rates for each reaction were plotted vs. ATP concentration and fitted to a Michaelis Menton (discussed further in Appendix B) curve to determine the catalytic rate constant, k_{cat}. The k_{cat} values were used to produce an Eyring plot to determine biochemical characteristics.

Results

Rok1p (+) RNA

Initial experiments with Rok1p had suggested that two rate limiting steps occurred at different temperatures. In order to confirm this hypothesis more trials were required to determine the statistical variability. A malachite green-ammonium molybdate assay was used to obtain these trials. The malachite green assay utilizes the color change associated with the coordination of phosphate with molybdate to form a phosphomolybdate complex.[48,49] The ionic interaction of malachite green with the anionic phosphomolybdate complex is responsible for the color change from yellowish-green to dark blue-green. This color change was monitored through absorbance readings using an infinite M200 spectrophotometer and the program Magellan®.

A phosphate standard curve was necessary in order to determine the amount of phosphate present in the reactions with Rok1p (Figure 15). To ensure a standard set up in regards to absorbance, the buffer for the phosphate standard curve was the same as that used in the reactions minus protein and RNA. A phosphate standard calibration curve was produced for every assay.

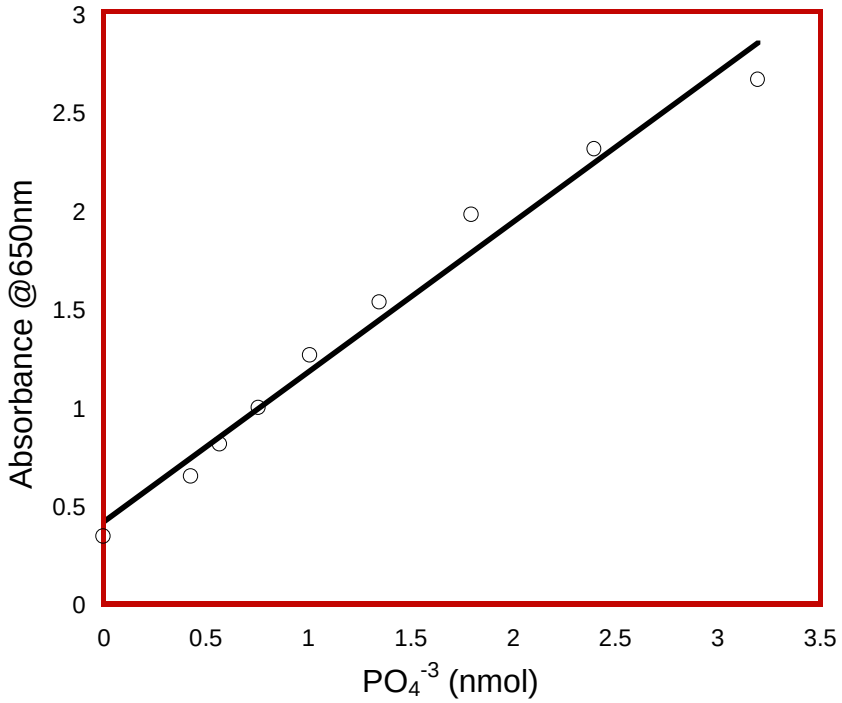


Figure 15: An example of the phosphate standard calibration curve. Every phosphate standard calibration curve possessed an R^2 value ≥ 0.99.

The initial data analysis determined the amount of phosphate detected over the 8 time points (Figure 16).

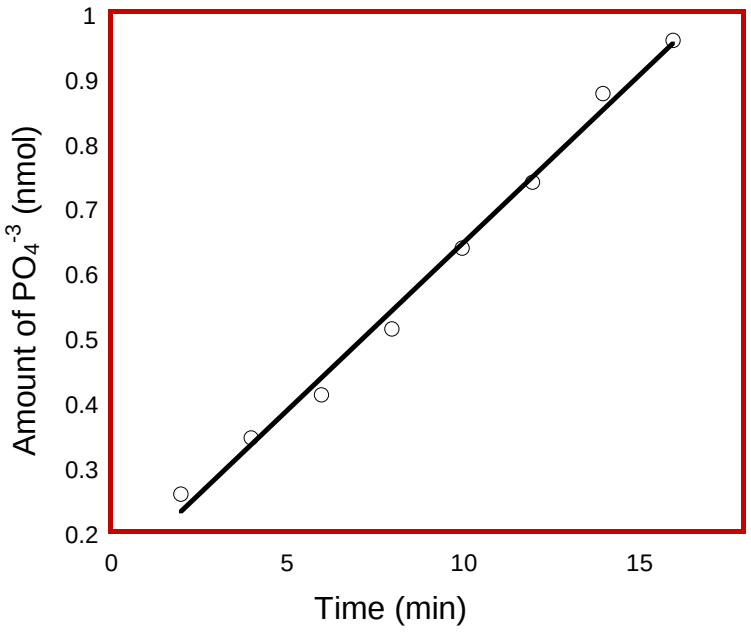


Figure 16: Amount of phosphate (nmol) detected for a Rok1p assay at 18°C in the presence of RNA using the 0.67mM ATP reaction.

The slope of the linear fit in Figure 16 was used to determine the rate of each reaction at various ATP concentrations. The rates of each reaction were fit to a Michaelis Menton curve to obtain the catalytic rate constants (k_{cat}) and the binding constants (K_M) (Figure 17).

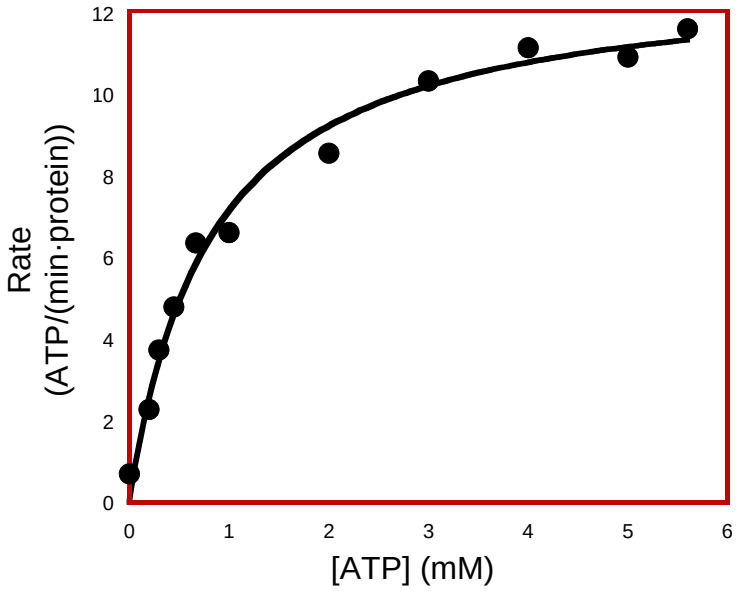


Figure 17: ATPase activity of Rok1p in the presence of RNA at 38°C with a Michaelis Menton curve fit. The k_{cat} is 12.975min^{-1} and the K_M is 0.81629mM.

The assays were run twice at each temperature in order achieve a total of three trials; one trial by Geno Raggi and two trials by Robert Carlisle. The average of the three catalytic rate constants determined from the Michaelis Menton curves were used to produce the Eyring plot below (Figure 18):

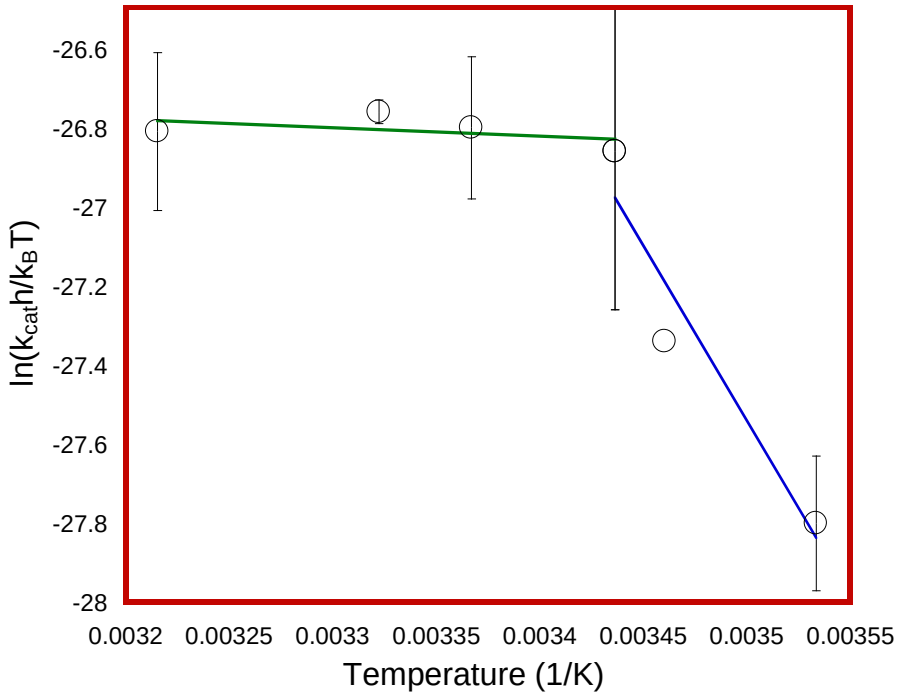


Figure 18: The Eyring plot of Rok1p in the presence of RNA. The linear fit error bars signify the standard deviation of three trials. One trial at each temperature was performed by Geno Raggi[37] and the remaining trials were carried out by Robert Carlisle.

The thermodynamic parameters for the high (24-38°C) and low (10-18°C) temperature ranges were elucidated from Figure 18 and displayed in Table 7 below:

Table 7: Thermodynamic parameters of each state of Rok1p in the presence of RNA.

Temp Range (°C)	**$\Delta H^{\ddagger}$ (kJ/mol)**	**$\Delta S^{\ddagger}$ (kJ/mol K)**
10-18	73.76	0.0292
24-38	1.74	-0.217

The extremely large $\Delta H^{\ddagger}$ at low temperatures, 73.76kJ/mol, is representative of a great deal of bonds breaking, thus supporting a preexisting closed ordered conformation. Energy must be inputted to disrupt the intermolecular forces. The dissolution and formation of intermolecular forces between the two RecA-like domains of Rok1p in order to accommodate ATP most likely

contributes to the enthalpic value. Furthermore, since RNA is present, there could be intermolecular forces between the protein and the RNA that need to be rearranged in order to accommodate ATP and RNA binding. However, it is unknown how much of the enthalpic value represents the binding of RNA or the binding of ATP.

Further support for the closed ordered conformation can be found in the $\Delta S^{\ddagger}$ (Table 7). Positive entropy means that there is an increase in disorder in the system at the transition state. Generally, a transition state is more ordered than the reactants, represented by negative entropy. Prior to the transition state the Rok1p active site is in an ordered state with a complex network of hydrogen bonds and other intermolecular forces. The insertion of ATP into the active site disrupts some of these interactions. Even though ATP is bound via hydrogen bonds, there may be a less complex network of interactions in the transition state, thus the slight increase in entropy.

Conversely, the negative entropy of the transition state over the 24-38°C temperature range signifies Rok1p becoming more ordered (Table 7). The reactant, Rok1p, is in a disordered state because the increased temperature disrupts the intermolecular forces that keep the protein in an ordered state. The binding of ATP facilitates the closing of Rok1p and the formation of a complex network of hydrogen bonds between the two RecA-like domains as well as with ATP, thus increasing order and decreasing entropy. At higher temperatures in the presence of RNA, Rok1p must first get itself into the closed conformation and then bind ATP.

Although the enthalpy at higher temperatures is positive, the magnitude is minute in comparison to the lower temperatures, thus providing evidence of an open disordered conformation (Table 7). Energy is given off when bonds are formed. In order to get into the appropriate conformation to bind ATP, Rok1p must form some intermolecular forces to bring the

two domains together thus releasing energy. Although these intermolecular forces contribute to the net $\Delta H^{\ddagger}$, they are not able to overcome all the bonds that must be broken, possibly bonds between RNA base pairs, in order to bind with Rok1p.

The aforementioned results suggest that in the presence of RNA, Rok1p displays biphasic character for the catalytic step.

Dpb3p (-) RNA

Like Rok1p, Dbp3p is also a DEAD-box protein involved with yeast ribosomal biogenesis. As previously mentioned, Dbp3p exhibited ATPase activity in the absence of RNA, also similar to Rok1p. These similarities made Dbp3p a prime candidate for determining whether or not characteristics displayed by Rok1p in the absence of RNA were unique or common to all DEAD-box proteins.

There were multiple aspects of the assay that were adjusted in order to obtain accurate results for Dbp3p in the absence of RNA. Several problems arose because of the sensitive nature of the assay and Dbp3p, the first being achieving saturation (Figure 19), thus high ATP concentrations were analyzed. The Michaelis Menton curve for Dbp3p activity at 18°C used the same ATP dilution as Rok1p (Figure 19). However, at higher concentrations the absorbances were above the detection limits of the detector even at the first time point. It is possible that the ATP stock utilized began to degrade into ADP and P_i thus increasing the background rate. Multiple ATP aliquots were tested and each yielded negative results.

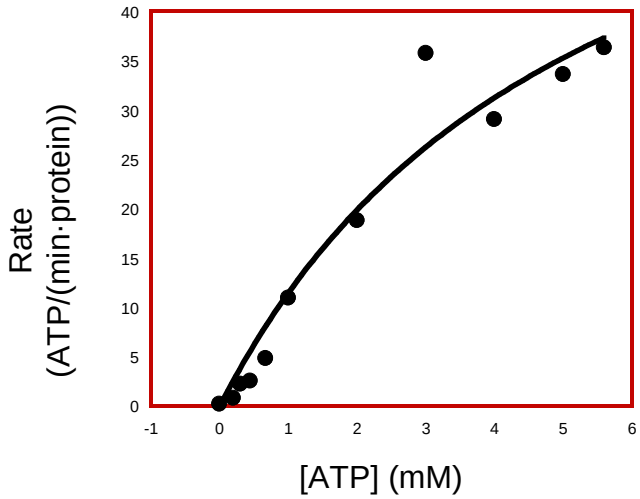


Figure 19: Michaelis Menton curve of Dbp3p at 18°C in the absence of RNA. The ATP dilution started at 5.60mM and yielded a k_{cat} of 73.18min^{-1}·$protein^{-1}$ and a K_M of 5.34mM.

Using freshly made ATP and starting the ATP dilution at 6mM resulted in achieving saturation at 18°C (Figure 20). However, the reactions consisting of 5.37 and 6.0mM ATP reached completion quickly and did not provide enough data to determine a rate. The Michaelis Menton curve highlights the latter stages of the reaction and saturation, evident by the flattened curve at the higher ATP concentrations; this flattened portion is lacking in Figure 19.

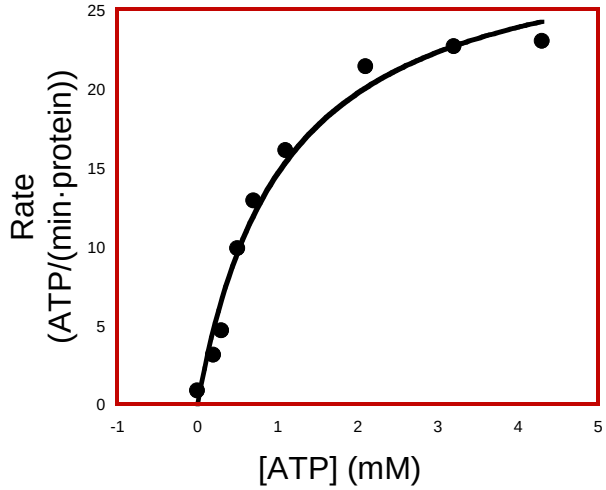


Figure 20: Michaelis Menton curve for Dbp3p assay at 18°C in the absence of RNA using the modified incubation schedule. The first two reaction rates have been omitted. The k_{cat} is 30.35min^{-1}·$protein^{-1}$ and the K_M is 1.07mM.

Multiple reaction conditions were adjusted in attempts to resolve the issues seen with the higher ATP concentrations. The incubations of the well-plate were adjusted from the original;

the first 15 minute incubation was split into three 5 minute incubations to obtain more absorbance readings for the higher ATP concentrations, but the two subsequent 10 minute incubations were unchanged (Table 8, condition 1). In an effort to accommodate the faster reaction rates of Dbp3p, the time points were shortened (Table 8, condition 2). It was also hypothesized that using a Mg^{2+}/Hepes buffer for ATP dilutions would help to stabilize the ATP (Table 8, condition 3). The ATP dilution procedure was reexamined to no avail (Table 8, condition 4). It was thought that the technique used in the ATP serial dilution of the highest two ATP concentrations was causing the problem. Since EDTA is responsible for the stopping the reaction, via coordination to Mg^{2+}, increasing its 1X concentration from 125mM to 250mM was thought to stop the reaction more efficiently and prevent the extremely fast rates (Table 8, condition 5). None of the above adjustments significantly improved the results. It is very important to determine the rates for the higher ATP concentrations in order to create an accurate assessment of Dbp3p over the specified temperature range.

Table 8: Average rates of each reaction for the various assay adjustments. (1) Modified Incubation Schedule (2) Shortened Time Points (3) Mg^{2+}/Hepes Buffer (4) ATP Dilution Process (5) Increased EDTA Concentration All assays were performed using the modified incubations. * ATP serial dilution 6.09, 4.6, 3.0, 1.5, 1.0, 0.7, 0.5, 0.3, 0.2, 0.1, and 0mM. **(2) used the original incubations: 15, 10, and 10 minute incubations at 35°C.

ATP Concentration (mM)	Original Conditions	1	2**	3	4*	5
6.00	36.42	-37.22	-23.50	-45.88	6.51	-0.17
5.37	33.70	7.81	30.92	-73.97	0.33	1.16
4.30	29.12	23.04	82.80	-31.09	26.38	2.35
3.20	35.83	22.70	70.06	-17.85	34.79	0.26
2.10	18.86	21.43	43.20	-19.67	40.61	0.07
1.10	10.99	16.12	29.33	-14.49	21.15	1.57
0.70	4.87	12.90	28.95	20.38	19.12	-0.97
0.50	2.54	9.88	14.25	14.18	9.49	0.52
0.30	2.23	4.66	5.89	8.58	7.27	-0.62
0.20	0.81	3.11	5.56	7.55	3.78	2.32
0.00	0.21	0.85	0.00	0.00	1.87	1.83

Although the modified incubation schedule did not solve the issues with the higher ATP concentrations by itself, it did provide more data for each reaction (Table 8). The extra absorbance readings provided more rates that could be averaged to obtain a more accurate rate. Shortening the time points for the higher ATP concentrations still yielded a negative rate (6.00) and multiple rates that were very fast (4.30, 3.20, 2.10). This fact indicated that something else was causing the negative rates. The Mg^{2+}/Hepes buffer for the ATP serial dilution exacerbated the negative rate problem. There may have been more interactions than normal of Mg^{2+} with the protein that could have hindered its ATPase activity. Adjusting the ATP dilution process was unsuccessful. The 2.10mM reaction, 1/3 the concentration of highest concentration, had a rate that was more than 6-fold greater than the 6.00mM reaction. The results obtained from increasing the EDTA 1X concentration showed rates that hovered around zero. This suggested

that the added EDTA may have interacted with the protein such that it almost abolished Dbp3p's ATPase activity (Table 8).

Because changing the assay conditions did not resolve the problem, each component in the reaction was tested. All the reagents in the reaction mixture were tested to determine if they had PO_4^{-3} contamination or if there was a threshold at which they disrupted the phosphate detecting agent (Figure 21).

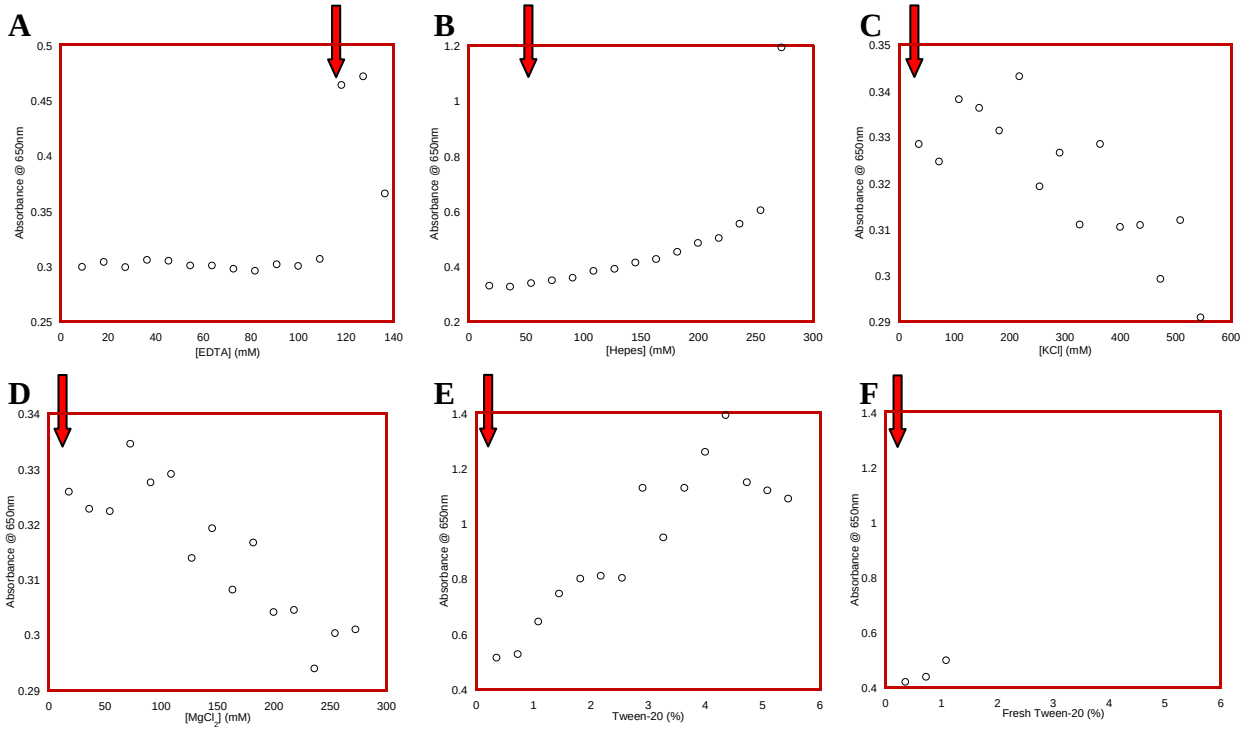


Figure 21: Absorbances at 650nm of various 1.25X components. (A) EDTA (B) Hepes (C) KCl (D) $MgCl_2$ (E) Tween-20 (F) Fresh Tween-20 The red arrow indicates approximately the 1X concentration used for the Rok1p and Dbp3p assays.

Although KCl and $MgCl_2$ showed a general decrease in absorbance as their concentration increases, a closer examination of the range in which the data points occupy indicated that the absorbance stays fairly constant regardless of absorbance (Figure 21C and D, respectively). This suggested that the background absorbance for the phosphate detecting agent was between 0.3 and 0.4. The data also illustrated that absorbance readings steadily increased at higher concentrations

for Hepes (Figure 21B). However, the 1X concentration used in the reactions was 50mM. The absorbance at this concentration was approximately 0.35, close to the background absorbance of the phosphate detecting agent. The increased absorbance with increased concentration of Tween-20 suggested that it must have degraded overtime (Figure 21E). Fresh 25% Tween-20 was made and the subsequent assay yielded the following Michaelis Menton curve which illustrates a saturation rate at higher concentration (Figure 22).

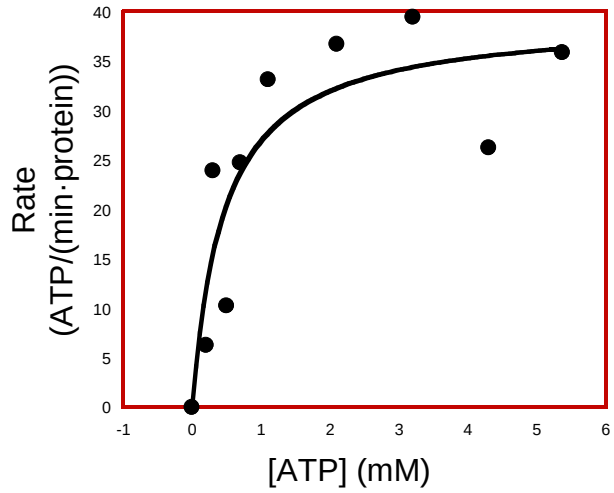


Figure 22: Michaelis Menton curve for Dbp3p assay at 24°C in the absence of RNA using fresh 25% Tween-20. The first reaction rate has been omitted. The catalytic rate constant is 39.40min^{-1}·$protein^{-1}$ and the Michaelis constant is 0.46mM.

The k_{cat} values determined from the aforementioned Michaelis Menton curves were then plotted using an Eyring plot. The Eyring plot relates the rates to temperature and allows thermodynamic parameters representative of the transition state to be determined. An Eyring plot of Dbp3p and Rok1p in the absence of RNA is shown below in Figure 23.

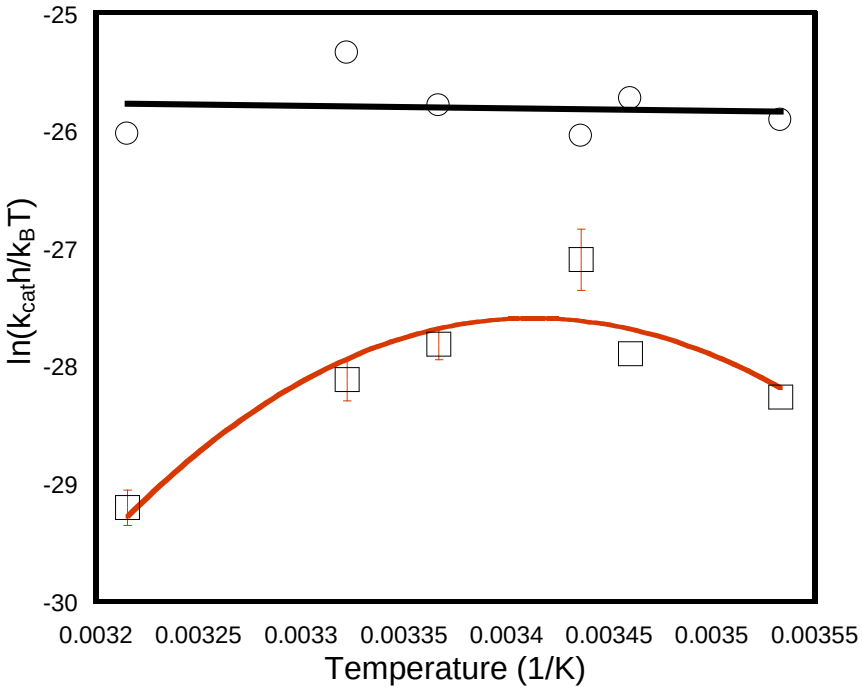


Figure 23: Eyring plot of Dbp3p (circles) and Rok1p (squares) in the absence of RNA. The data for Rok1p was collected by Geno Raggi.[37] The Dbp3p data is fit linearly while Rok1p is fit to the integrated Eyring equation (see Equation 2) The error bars signify the standard deviation of three trials.

Unlike Rok1p, temperature and rate exist in a linear relationship for Dbp3p (Figure 23). In general, the rate increases with increasing temperature. Dbp3p possesses a large $\Delta H^{\ddagger}$ of 1.81kJ/mol in the absence of RNA suggesting that a lot of bonds are being broken within the protein. The -0.208kJ·mol^{-1}·K^{-1} $\Delta S^{\ddagger}$ value means the transition state is more ordered than the reactants; Dbp3p goes from an open disordered conformation to a closed conformation in order to bind ATP.

The above results suggest that Dbp3p favors an initially open disordered conformation and its ATPase activity is directly proportional to temperature.

Dbp3p (+) RNA

Although Dbp3p possesses higher catalytic rates than Rok1p, the two proteins are very similar. Their similar functions in yeast ribosomal biogenesis motivate comparative research to

determine if the possible biphasic nature displayed by Rok1p is also present in Dbp3p. If so, this biochemical trait may be shared across all DEAD-box proteins.

The same conditions that yielded measureable data for Dbp3p in the absence of RNA were used for Dbp3p in the presence of RNA. However, these results produced rates too fast to measure giving apparently negative rates because the reaction reached completion so quickly. Instead of measuring the actual rate of reaction, the rate of saturation was being measured. It is probable that when a small portion of data at saturation is examined a negative rate results. Because the issues arose sporadically at various ATP concentrations, adjusting the time points would not have been useful; there was a global issue with the assay conditions.

The negative rates and extremely fast rates led to additional troubleshooting with glycerol, diluted reactions, filtered phosphate detecting agent, and the integrity of the components in the 1.25X Master Mix. Since the stock concentration of Dbp3p was greater than Rok1p, less glycerol was present in the Dbp3p assays. It was hypothesized that glycerol may interact with the protein to prevent the negative and extremely fast rates. Thus, glycerol was added to the 1.25X Master Mix to test this hypothesis. Another strategy involved diluting the final reactions through the addition of 50% more phosphate detecting agent. If there were interactions between the reaction components such as Mg^{2+}, K^{+}, or Cl^{-} and the molybdate that inhibited phosphate coordination, the added phosphate detecting agent would still be able to capture phosphate. Precipitates were noticed in the 384-well plate days after assays had been performed. Filtering these precipitates was thought to prevent any negative interactions that could occur with the protein. The components of the 1.25X Master Mix were examined individually for residual phosphate or degradation; nine separate 1.25X Master Mixes were produced. The first 1.25X Master Mix consisted of only ddH_2O, the second had ddH_2O and 25%

Tween-20, the third had ddH_2O, 25% Tween-20, and Hepes, etc. Another component was added to each subsequent 1.25X Master Mix until the ninth one had all the components outlined in the methods.

Although the addition of glycerol did not vastly improve the results, it was kept in the reaction mixture to ensure consistency with Rok1p assays. Diluting the reactions with more phosphate detecting agent did rid the results of negative rates, but it did nothing to reign in the fast rates. The assay became extremely sensitive upon filtering the phosphate detecting agent, so sensitive that differences in phosphate concentrations were indistinguishable between the highest and lowest concentrations of ATP.

The examination of the components in the 1.25X Master Mix did show positive results. The average rates for the reactions without Dbp3p were non-zero values (Figure 24, 1.25X Master Mixes 1-7). This suggests that the combination of the reaction mixture may degrade the ATP, not the individual components. Additionally, in the process of examining the components, the order was modified such that the last three components added in order were glycerol, Dbp3p, and RNA. This order of addition showed markedly improved rates (Figure 24, 1.25X Master Mix 9). The rates for 1.25X Master Mix 9 varied from 57 to 68$min^{-1}\cdot protein^{-1}$, a tight range when compared to all other mixtures. A narrow range of rate for each absorbance reading reflects consistency in the protein; operating at its peak capacity for this particular ATP concentration. Data sets with a wide range of column heights are representative of abnormal protein activity; lacking certain 1.25X Master Mix components prevents some positive interactions with the protein (1.25X Master Mixes 1-8). The protein may have a rate of 30.31$ATP\cdot min^{-1}\cdot protein^{-1}$ and after another incubation period the rate has all of a sudden doubled to 62.36$ATP\cdot min^{-1}\cdot protein^{-1}$ (Figure 24; 1.25X Master Mix 5; incubation 3 and 4, respectively). The negative columns

displayed in 1.25X Master Mix 1 and 2 are also considered abnormal (Figure 24). This would mean that phosphate is being taken out of the mixture as time progreses.

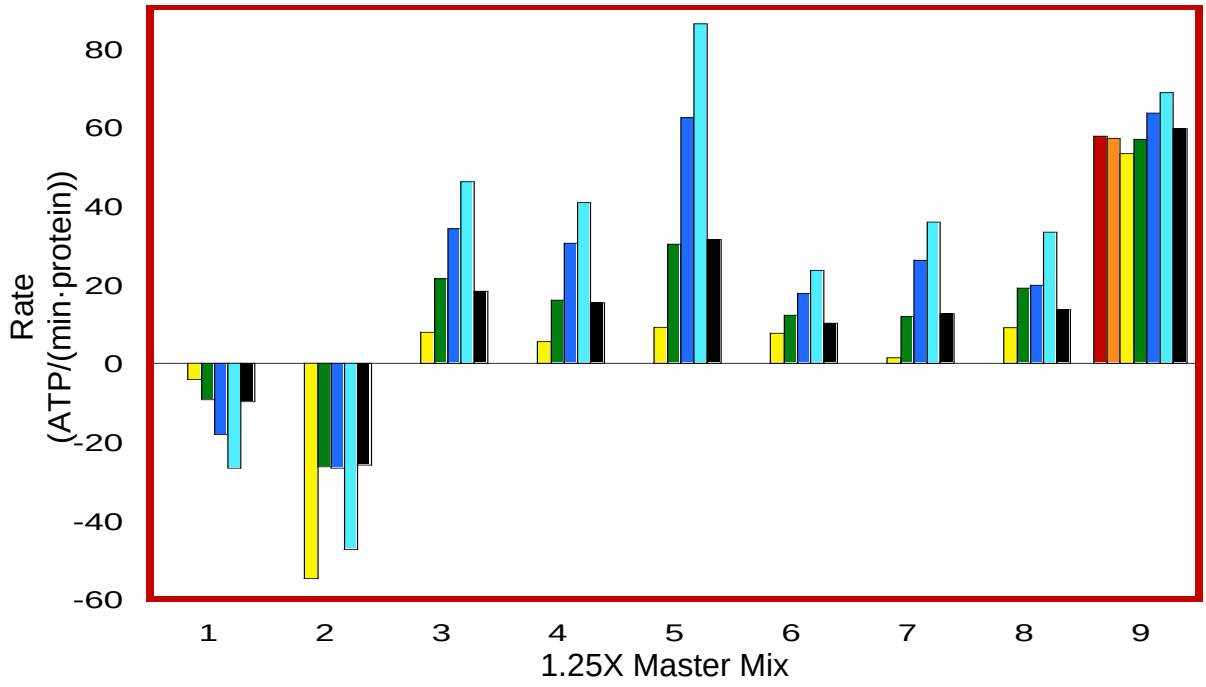


Figure 24: ATPase activity of various 1.25X Master Mixes in the presence of RNA. The numbers 1-9 refer to the 1.25X Master Mixes: (1) only ddH_2O; (2) ddH_2O and 25% Tween-20; (3) ddH_2O, 25% Tween-20, and Hepes; (4) ddH_2O, 25% Tween-20, Hepes, and KCl; (5) ddH_2O, 25% Tween-20, Hepes, KCl, and $MgCl_2$; (6) ddH_2O, 25% Tween-20, Hepes, KCl, $MgCl_2$, and DTT; (7) ddH_2O, 25% Tween-20, Hepes, KCl, $MgCl_2$, DTT, and 80% glycerol; (8) ddH_2O, 25% Tween-20, Hepes, KCl, $MgCl_2$, DTT, 80% glycerol, and Dbp3p; (9) ddH_2O, 25% Tween-20, Hepes, KCl, $MgCl_2$, DTT, 80% glycerol, Dbp3p, and RNA. The assortments of colors correspond to the rate determined from a specific incubation period: pre-incubation (red), incubation 1 (orange), incubation 2 (yellow), incubation 3 (green), incubation 4 (blue), or incubation 5 (indigo). The black columns represent the average rate of the reaction corresponding to a specific 1.25X Master Mix. Data sets missing columns did not have data to show for those particular incubations because the absorbances were either too high or low for the detector.

Lastly, the EDTA concentration was adjusted. It was previously determined that increasing the EDTA concentration made things worse suggesting that there may also be negative interactions with the reagent and Dbp3p. Figure 21A suggests that lowering the EDTA

concentration will not affect the absorbance anymore than the phosphate detecting agent. In an attempt to alleviate any of these negative interactions the EDTA 1X concentration was decreased to 75mM and reanalyzed. The data seemed to be consistent within all incubation periods and gave no negative values (Figure 25A). The Michaelis Menton curve clearly levels off as the ATP concentration increases, signifying that saturation has been reached. The presence of RNA at 10°C stimulates Dbp3p's k_{cat} two-fold from 34.86 to 63.12min^{-1}·$protein^{-1}$. This rate is faster than any other Dbp3p assay in the absence of RNA. The K_M value is not affected nearly as much, 0.38 to 0.42mM. The increase in the Michaelis constant suggests that ATP is not bound as tightly in the presence of RNA. However, the K_M value for Dbp3p in the absence of RNA was determined from a Michaelis Menton curve omitting three data points from higher ATP concentrations because of negative values (Figure 25B). These omissions could have flattened out the curve prematurely, resulting in the lower K_M value. More trials at 10°C in the presence and absence of RNA using the modified conditions need to be performed in order determine if the difference between K_M values is significant or negligible.

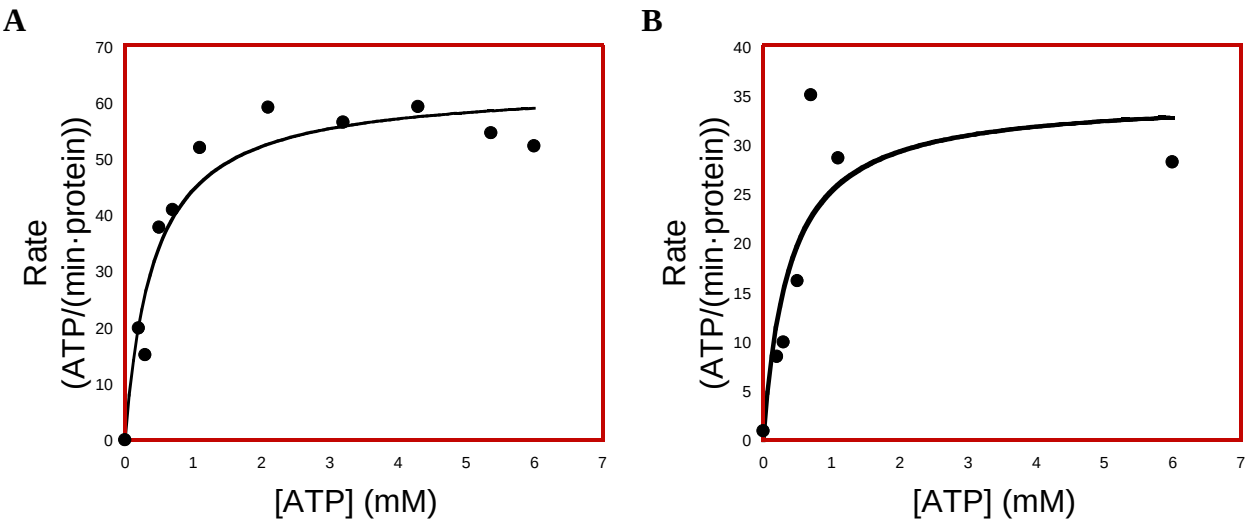


Figure 25: (A) Michaelis Menton curve for Dbp3p assay at 10°C in the presence of RNA using an EDTA 1X concentration of 75mM. The catalytic rate constant is 63.12min^{-1} and the Michaelis constant is 0.42mM. (B) Michaelis Menton curve for Dbp3p assay at 10°C in the absence of RNA. The catalytic rate constant is 34.86min^{-1} and the Michaelis constant is 0.38mM.

Conclusions

Rok1p Thermodynamics

In the presence of RNA, Rok1p produced a non-linear Eyring plot (Figure 18). The addition of error bars suggests that the break in the Eyring plot around 20°C is accurate and not simply an anomaly produced from one trial at each temperature. The break in the line corresponds to the transition seen in the absence of RNA (Figure 13). This illustrates that the open and closed conformations yield different rate limiting steps during the reaction. For example, the open state rate limiting step may be a combination of achieving the closed state as well as the chemistry involved with hydrolysis. The closed state rate limiting step may only be the hydrolysis chemistry.

This hypothesis is supported with thermodynamic data as well. The large positive enthalpy at lower temperatures signifies a great deal of bond breakage associated with ATP binding. Although the enthalpy at the higher temperatures was positive, numerous bonds are being formed to achieve a closed conformation, accounting for the extremely small magnitude. The barely positive entropy over the 10-18°C range suggests that the intermolecular interactions occurring at the transition state yield a slightly more disordered transition state compared to the reactants. The negative entropy associated with the 24-38°C range elucidates the opposite conclusion. The transition state is slightly more ordered than the unbound protein. The aforementioned data all support the hypothesis that Rok1p is a biphasic protein in the presence of RNA and exists in a disordered-ordered equilibrium in the absence of RNA.

Dbp3p Thermodynamics

Unlike Rok1p, Dbp3p exhibits a linear relationship between temperature and rate in the absence of RNA (Figure 23). In general, as the temperature increases so does the rate. This trend

adheres to the common chemistry principle: increasing temperature increases the average kinetic energy of the system, therefore making it more likely for a reaction to occur and subsequently increasing the rate of the reaction. The linear relationship also suggests that Dbp3p exists in a single state, in which there is one rate-determining step with constant activation energy. Of course, more trials at each temperature are needed in order to confirm the preliminary hypothesis. The thermodynamic parameters determined from the linear Eyring plot support another standard chemistry principle. As a reaction progresses from reactants to products it must first pass through a transition state. In order for the appropriate chemistry to occur the transition state becomes more ordered than the reactants. The negative entropy value characteristic of the linear relationship displayed in Figure 23 elucidates this common trait among all reactions. Dbp3p possessing a $\Delta S^{\ddagger}$ of -0.208 $kJ \cdot mol^{-1} \cdot K^{-1}$ indicates that the transition state of binding and hydrolyzing ATP is more ordered that the free Dbp3p protein. The entropy for Dbp3p is also similar to Rok1p at high temperatures (Table 7). This suggests that Dbp3p predominates in the open conformation.

The positive enthalpy value associated with the linear Eyring plot is more complex. As previously mentioned, all DEAD-box proteins exist in an ordered-disordered equilibrium and they generally favor the disordered state. The large positive enthalpy suggests that the open state of Dbp3p requires the rearrangement of many intermolecular forces within the protein unlike Rok1p. Thus, the equilibrium shift to a closed ordered conformation in the absence of RNA is unique to Rok1p. Considering Dbp3p and Rok1p do not exist in similar states in the absence of RNA, it can be hypothesized that Dbp3p will not exhibit two separate rate limiting steps like Rok1p. It is highly probable that Dbp3p, while in an open disordered conformation, will continue to display a directly proportional relationship between temperature and rate, although the rates

will probably be stimulated in the presence of RNA. The RNA will be able to facilitate the closing of Dbp3p so it can hydrolyze ATP more efficiently.

Appendix A

Derivation of Eyring Equation

The Eyring kinetics model treats the transition state of a reaction as a distinct intermediate therefore granting it thermodynamic parameters. The derivation of the Eyring equation and the integrated version are shown below:

$$R \rightleftharpoons R^{\ddagger} \rightarrow P$$

$$K_{eq}^{\ddagger} = \frac{R^{\ddagger}}{R} \qquad k^{\ddagger} = \frac{k_B T}{h} \qquad k_{obs} = \left(K_{eq}^{\ddagger}\right)\left(k^{\ddagger}\right)$$

$$\ln K_{eq}^{\ddagger} = \frac{-\Delta G^{\ddagger}}{RT} = \frac{-\Delta H^{\ddagger}}{RT} + \frac{\Delta S^{\ddagger}}{R}$$

$$\frac{d\Delta H^{\ddagger}}{dt} = \Delta C_p \implies \int_{T_0}^{T} d\Delta H^{\ddagger} = \int_{T_0}^{T} \Delta C_p dt \implies \Delta H^{\ddagger}(T) = \Delta H^{\ddagger}(T_0) + \Delta C_p(T - T_0)$$

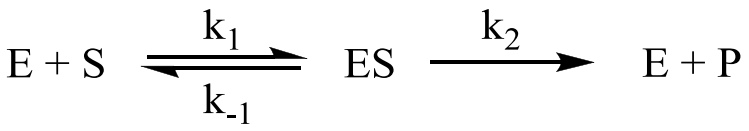
$$\frac{d\Delta S^{\ddagger}}{dt} = \frac{\Delta C_p}{T} \implies \int_{T_0}^{T} d\Delta S^{\ddagger} = \int_{T_0}^{T} \frac{\Delta C_p}{T} dt \implies \Delta S^{\ddagger}(T) = \Delta S^{\ddagger}(T_0) + \Delta C_p \ln\left(\frac{T}{T_0}\right)$$

$$\ln K_{eq}^{\ddagger} = \frac{-\Delta H^{\ddagger}(T_0)}{RT} + \frac{\Delta C_p(T - T_0)}{RT} + \frac{\Delta S^{\ddagger}(T_0)}{R} + \frac{\Delta C_p}{R}\ln\left(\frac{T}{T_0}\right) \implies$$

$$\ln\left(\frac{k_{obs} h}{k_B T}\right) = \frac{-\Delta H^{\ddagger}(T_0)}{RT} + \frac{\Delta S^{\ddagger}(T_0)}{R} + \frac{\Delta C_p}{R}\left(-1 + \frac{T}{T_0} + \ln\left(\frac{T}{T_0}\right)\right)$$

Appendix B

Michaelis Menton Kinetics



The four basic assumptions being made are as follows:

1. There is only one ligand, in this case ATP, and one binding site, in this case the active site of Rok1p or Dbp3p.
2. k_1 >>> k_2 therefore a rapid equilibrium is reached before substantial product formation
3. [S] >>> [E] therefore [ES] is considered a fixed concentration
4. Product formation is not reversible; k_{-2} is negligible

$$\frac{d[ES]}{dt} = 0 = k_1[E][S] - k_{-1}[ES] - k_2[ES]$$

$$[E]_{total} = [E] + [ES]$$

$$k_1([E]_{total} - [ES])[S] = (k_{-1} + k_2)[ES] \Rightarrow [ES](k_{-1} + k_2 + k_1[S]) = k_1[E]_{total}[S]$$

Divide both sides by k_1 and solve for [ES]

$$[ES] = \frac{[E]_{total}[S]}{K_M + [S]}$$

Where

$$K_M = \frac{k_{-1} + k_2}{k_1}$$

The initial velocity of the reaction is expressed as:

$$v_0 = \frac{dP}{dt} = k_2[ES]$$

Therefore:

$$v_0 = \frac{k_2[E]_{total}[S]}{K_M + [S]} = \frac{V_{max}[S]}{K_M + [S]} \; where \; V_{max} = k_2[E]_{total}$$

Furthermore $k_{cat} = \frac{V_{max}}{[E]_{total}} = k_2$

[1] Rocak, S., Linder, P. DEAD-box proteins: The Driving Forces Behind RNA Metabolism. *Nature* **2004**, 5: 232-240.
[2] peppy_pepz's world. http://peppy-pepz.blogspot.com/2008_11_01_archive.html (November 21, 2010).
[3] D'Adamo, P. The Individualist: A knowledgebase of biochemical individuality. http://www.drpeterjdadamo.com/wiki/wiki.pl?action=browse;oldid=DNA;id=Deoxyribonucleic_acid_(DNA) (November 21, 2010).
[4] Kalel, V. GeeK of Science: a nature network blog. http://blogs.nature.com/vishal/2010/05/solution_to_genome_special_quiz.html (November 21, 2010).
[5] Schroeder, R., Barta, A., Semrad, K. Strategies for RNA Folding and Assembly. *Nature* **2004**, 5: 908-919.
[6] Draper, D. E. Strategies for RNA folding. *Trends Biochem Sci.* **1996**, 4: 145-149.
[7] Kossen, K., Karginov, F. V., Uhlenbeck, O. C. The Carboxy-terminal Domain of the DExD/H Protein YxiN is Sufficient for Confer Specificity for 23 S rRNA. *J. Mol. Biol.* **2002**, 324: 625-636.
[8] Henn, A., Shi, S., Zarivach, R., Ben-Zeev, E., Sagi, I. The RNA Helicase DbpA Exhibits a Markedly Different Conformation in the ADP-bound State When Compared with the ATP- or RNA-bound States. *J. Biol. Chem.* **2002**, 277: 46559-46565.
[9] Cordin, O., Banroques, J., Tanner, N. K., Linder, P. The DEAD-box protein family of RNA helicases. *GENE* **2006**, 367: 17-37.
[10] Story, R. M., Steitz, T. A. Structure of the recA protein-ADP complex. *Nature* **1992**, 355: 374-376.
[11] Xing, X., Bell, C. E. Crystal Structures of *Escherichia coli* RecA in Complex with MgADP and MnAMP-PNP. *Biochemistry* **2004**, 43: 16142-16152.
[12] Walker, J. E., Saraste, M. J., Runswick, J. J., Gray, N. J. Distantly related sequences in the α- and β-subunits of ATPase, myosin, kinases and other ATP-requiring enzymes and a common nucleotide-binding fold. *EMBO J.* **1982**, 1: 945–951.
[13] Sengoku, T., Nureki, Osamu, Nakamura, A., Kobayashi, S., Yokoyama, S. Structural Basis for RNA Unwinding by the DEAD-Box Protein *Drosophila Vasa*. *Cell* **2006**, 125: 287-300.
[14] Dillingham, M.S., Soultanas, P., Wigley, D.B. Site-directed mutagenesis of motif III in PcrA helicase reveals a role in coupling ATP hydrolysis to strand separation. *Nucleic Acids Res.* **1999**, 27: 3310–3317.
[15] Story, R.M., Li, H., Abelson, J.N. Crystal structure of a DEAD box protein from the hyperthermophile *Methanococcus jannaschi*. *Proc. Natl. Acad. Sci. U. S. A.* **2001**, 98: 1465–1470.
[16] Shi, H., Cordin, O., Minder, C.M., Linder, P., Xu, R.M. Crystal structure of the human ATP-dependent splicing and export factor UAP56. *Proc. Natl. Acad. Sci. U. S. A.* **2004**, 101: 17628–17633.
[17] Caruthers, J.M., Johnson, E.R., McKay, D.B. Crystal structure of yeast initiation factor 4A, a DEAD-box RNA helicase. *Proc. Natl. Acad. Sci. U. S. A.* **2000**, 97: 3080–3085.
[18] Caruthers, J. M., McKay, D. B. Helicase structure and mechanism. *Curr. Opin. Struct. Biol.* **2002**, 12**:** 123-133.
[19] Oh, J., Kim, J. ATP Hydrolysis activity of the DEAD box protein Rok1p is required for *in vivo ROK1* function. *Nucleic Acids Research* **1999**, 27: 2753-2759.
[20] Ruggero, D., Grisendi, S., Piazza, F., Rego, E., Mari, F., Rao, P. H., Cordon-Cardo, C., Pandolfi, P. P. Dyskeratosis Congenita and Cancer in Mice Deficient in Ribosomal RNA Modification. *SCIENCE* **2003**, 299: 259-262.
[21] Ford, C. L., Randal-Whitis, L., Ellis, S. R. Yeast Proteins Related to the p40/Laminin Receptor Precursor Are Required for 20S Ribosomal RNA Processing the Maturation of 40S Ribosomal Subunits. *Cancer Research* **1999**, 59: 704-710.
[22] Grisendi, S., Mecucci, C., Falini, B., Pandolfi, P. P. Nucleophosmin and cancer. *Nature Reviews Cancer* **2006**, 6: 493-505.
[23] Ghoshal, K., Jacob, S. T. Specific Inhibition of Pre-Ribosomal RNA Processing in Extracts from the Lymphosarcoma Cells Treated with 5-Fluorouracil. *Cancer Research* **1994**, 54: 632-636.
[24] Wilkinson, D. S., Tlsty, T. D. Hanas, R. J. The Inhibition of Ribosomal RNA Sythesis and Maturation in Novikoff Hepatoma Cells by 5-Fluorouridine. *Cancer Research* **1975**, 35: 3014-3020.
[25] Kressler, D., Linder, P., de la Cruz, J. Protein *trans*-Acting Factors Involved in Ribosome Biogenesis in *Saccharomyces cerevisiae*. *Molecular and Cellular Biology* **1999**, 19: 7897-7912.
[26] Leary, D. J., Huang, S. Regulation of ribosome biogenesis within the nucleolus. *FEBS Letters* **2001**, 509: 145-150.

[27] Lafontaine, D. L. J., Tollervey, D. Birth of the snoRNPs: the evolution of the modification-guide snoRNAs. *Trends Biochem Sci.***1998**, 23: 383-388.
[28] Venema, J., Bousquet-Antonelli, C., Gelugne, J., Caizergues-Ferrer, M., Tollervey, D. Rok1p Is a Putative RNA Helicase Required for rRNA Processing. *Molecular and Cellular Biology* **1997**, 17: 3398-3407.
[29] Balakin, A. G., Smith, L, Fournier, M. J. The RNA World of the Nucleolus: Two Major Families of Small RNAs Defined by Different Box Elements with Related Functions. *Cell* **1996**, 86: 823-834.
[30] Garcia, I., Uhlenbeck, O. C. Differential RNA-Dependent ATPase Activities of Four rRNA Processing Yeast DEAD-Box Proteins. *Biochemistry* **2008**, 47: 12562-12573.
[31] Karginov, F. V. Caruthers, J. M., Hu, Y, McKay, D. B., Uhlenbeck, O. C. YxiN Is a Modular Protein Combining a DExD/H Core and a Specific RNA-binding Domain. *J. Biol. Chem.* **2005**, 280: 35499-35505.
[32] Grohman, J. K., Campo, M. D., Bhaskaran, H., Tijerina, P., Lambowitz, A. M., Russell, R. Probing the Mechanisms of DEAD-Box Proteins as General RNA Chaperones: The C-Terminal Domain of CYT-19 Mediates General Recognition of RNA. *Biochemistry* **2007**, 47: 3013-3022.
[33] Mohr, G., Campo, M. D., Mohr, S., Yang, Q., Jia, H., Jankowsky, E., Lambowitz, A. M. Function of the C-terminal Domain of the DEAD-Box Protein Mss116p Analyzed *In Vivo* and *In Vitro*. *J. Mol. Biol.* **2008**, 375: 1344-1364.
[34] Keramisanou, D., Biris, N., Gelis, I., Sianidis, G., Karamanou, S., Economou, A., Kalodimos, C. G. Disorder-order folding transitions underlie catalysis in the helicase motor of SecA. *Nature Structural & Molecular Biology* **2006**, 13: 594-602.
[35] Kumaran, S., Grucza, R. A., Waksman, G. The tandem Src homology 2 domain of the Syk kinase: A molecular device that adapts to interphosphotyrosine distances. *PNAS* **2003**, 100: 14828-14833.
[36] Grucza, R. A., Futterer, K., Chan, A. C., Waksman, G. Thermodynamic Study of the Binding of the Tandem-SH2 Domain of the Syk Kinase to a Dually Phosphorylated ITAM Peptide: Evidence for Two Conformers. *Biochemistry* **1999**, 38: 5024-5033.
[37] Raggi, E. P. A Thermodynamic Analysis of the DEAD-box RNA helicase Rok1p. Allegheny College Senior Comprehensive Project, **2010** Editor: Dr. Ivelitza Garcia
[38] Truhlar, D. G., Kohen, A. Convex Arrhenius plots and their interpretation. *PNAS* **2001**, 98: 848-851.
[39] Labrou, N. E., Kotzia, G. A., Clonis, Y. D. Engineering the xenobiotic substrate specificity of maize glutathione S-transferase I. *Protein Engineering, Design & Selection* **2004**, 17: 741-748.
[40] De Mol, N. J., Dekker, F. J., Broutin, I., Fischer, M. J. E., Liskamp, R. M. J. Surface Plasmon Resonance Thermodynamic and Kinetic Analysis as a Strategic Tool in Drug Design. Distint Ways for Phosphopeptides to Plug into Src- and Grb2 SH2 Domains. *J. Med. Chem.* **2005**, 48: 753-763.
[41] Kil, Y. V., Glazunov, E. A., Lanzov, V. A. Characteristic Thermodependence of the RadA Recombinase from the Hyperthermophilic Archaeon *Desulfurococcus amylolyticus*. *J. Bacteriology* **2005**, 187: 2555-2557.
[42] Spies, M., Kil, Y., Masui, R., Kato, R., Kujo, C., Ohshima, T., Kuramitsu, S., Lanzov, V. The RadA protein from a hyperthermophilic archaeon *Pyrobaculum islandicum* is a DNA-dependent ATPase that exhibits two disparate catalytic modes, with a transition temperature at 75°C. *Eur. J. Biochem.* **2000**, 267: 1125-1137.
[43] Amutha, B., Khire, J. M., Khan, M. I. Characterization of a novel exo-*N*-acetyl-β-D-glucosaminidase from the thermotolerant *Bacillus* sp. NCIM 5120. *Biochemica et Biophysica Acta* **1998**, 1425: 300-310.
[44] Caglio, R., Valetti, F., Caposio, P., Gribaudo, G., Pessione, E., Giunta, C. Fine-Tuning of Catalytic Properties of Catechol 1,2-Dioxygenase by Active Site Tailoring. *ChemBioChem* **2009**, 10: 1015-1024.
[45] Hsuanyu, Y., Wedler, F. C., Kantrowitz, E. R., Middleton, S. A. Site-specific Mutation of Tyr^{240}→ Phe in the Catalytic Chain of *Escherichia coli* Aspartate Transcarbamylase. *J. Biol. Chem.* **1989**, 264: 17259-17265.
[46] Ferro, A. Masson, P. Kinetic evidence for thermally induced conformational change of butyrylcholinesterase. *Biochemica et Biophysica Acta* **1987**, 916: 193-199.
[47] Weaver, P. L., Sun, C., Chang, T. Dbp3p, a Putative RNA Helicase in *Saccharomyces cerevisiae*, Is Required for Efficient Pre-rRNA Processing Predominantly at Site A_3. *Molecular and Cellular Biology* **1997**, 17: 1354-1365.
[48] Cogan, E. B., Birrell, G. B., Griffith, O. H. A Robotics-Based Automated Assay for Inorganic and Organic Phosphates. *Analytical Biochemistry* **1999**, 271: 29-35.
[49]Mok, M. T. S., Edwards, M. R. Critical sources of error in colorimetric assay for UDP-*N*-acetylglucosamine pyrophosphorylase. *Analytical Biochemistry* **2005**, 343: 341-343.